environments

MDPI

Article

Role of Clay Dispersion and Cation Transfer in Montmorillonite-Catalyzed Ozonation of Bisphenol A in Water Treatment and Induced Ecotoxicity

Ahlem Bargougui [1], David Dewez [1,2,*] and Abdelkrim Azzouz [1,3,*]

[1] Centre Recherche des Nanomatériaux (NanoQAM), Department of Chemistry, University of Quebec at Montreal, Montreal, QC H3C 3P8, Canada; bargougui.ahlem@courrier.uqam.ca
[2] Centre de Recherche en Toxicologie et Santé de L'environnement (TOXEN-EcotoQ), Department of Chemistry, University of Quebec at Montreal, Montréal, QC H3C 3P8, Canada
[3] Département de Génie de la Construction, École de Technologie Supérieure, Montréal, QC H3C 1K3, Canada
* Correspondence: dewez.david@uqam.ca (D.D.); azzouz.a@uqam.ca (A.A.);
Tel.: +1-514-987-3000 (ext. 3278) (D.D.); +1-514-987-3000 (ext. 4119) (A.A.)

Abstract

The effects of exchangeable cations on bisphenol A adsorption and degradation were investigated in montmorillonite-catalyzed ozonation and compared to the parent bentonite. Total BPA removal (100%) can be achieved after only 5 min adsorption on NaMt and by 15 min ozonation with all clay catalysts but without complete mineralization. The BPA degradation level was found to correlate to the ecotoxicity of the ozonized BPA mixtures, using the aquatic plant *Lemna minor* as a bioindicator species. Liquid chromatography revealed that BPA adsorption contributes to the ozonation process and that BPA degradation rates and ecotoxicity strongly depend on the exchangeable cation and the particle size of the clay catalyst. These factors also appear to govern the ozonation and adsorption process through catalyst dispersion in the liquid medium, with direct effects on the toxicity towards the living species. The results of the present work allow envisaging clay-based oxidative water treatments with advanced BPA removal that drastically reduce the amounts of persistent derivatives.

Keywords: montmorillonite; clay catalysts; ozonation; *Lemna minor*; ecotoxicity

Check for updates

Academic Editor: Roberta Bettinetti

Received: 13 April 2026
Revised: 2 May 2026
Accepted: 6 May 2026
Published: 9 May 2026

Copyright: © 2026 by the authors. Licensee MDPI, Basel, Switzerland. This article is an open access article distributed under the terms and conditions of the Creative Commons Attribution (CC BY) license.

1. Introduction

The presence of organic pollutants in aquatic environments unavoidably affects ecosystems, biodiversity, and human health. Their partial oxidation under ambient conditions is known to generate a diversity of intermediates; some of these can accumulate, leading to potential toxicity to aquatic life. Among key pollutants, bisphenol A (BPA), or 2,2-bis-(4-hydroxyphenyl) propane, is commonly detected in various wastewaters due to its widespread use as an additive in manufacturing epoxy resins and polycarbonate plastics [1], mostly for packaging food, drugs, cosmetics, and others [2,3]. BPA concentrations ranging from 10 to 1000 ng·L^{-1} were already reported in surface waters [4], even exceeding 10–20 µg·L^{-1} in industrial and urban wastewaters [5,6]. Despite imposed water quality requirements, BPA persists at concentrations of up to 1 µg·L^{-1} in treated waters [7] and even 2 ng·L^{-1} in drinking water [8], being detected in foods, human tissues, and liquids [9–11].

The effects of the long-term exposure of human consumption products to BPA and the slow and inevitable degradation of BPA into intermediates in air-exposed

natural media remain unknown. The rise of more or less harmful derivatives contributes to the ecotoxicity impact in nature, with unknown consequences for the environment and biodiversity [12–19]. BPA is a well-documented endocrine-disrupting compound (EDC). BPA was found to affect the hormonal and animal reproduction systems of aquatic ecosystems [20–22], causing the pronounced feminization of some aquatic species [23–25], fertility issues [26], embryo implantation decay [27], and valvulocardiovascular pathologies [28,29]. Exposure to BPA has also been associated with reduced growth for *Lemna minor* and increased toxicity for *Artemia salina* [30]. BPA was found to trigger some cancers [31], high blood pressure, heart disease, diabetes, prostate cancer cells, and liver dysfunction in humans [32,33]. Human health requirements have resulted in a ban on the use of BPA in the manufacture of baby utensils since 2011 [26,34,35].

BPA has a chemical structure with phenolic groups that confer stability against mild oxidants and persistence in air-exposed environments, hindering complete mineralization [1]. Moreover, the amphoteric-to-slightly-basic character is expected to confer high stability to BPA at acidic and basic pHs, which mitigates its natural degradation [36]. Even in the presence of UV–vis radiation and oxidants such as ozone (O_3), BPA oxidation in nature is often incomplete, resulting in degradation products that can still cause additional cellular damage in aquatic organisms by disrupting their antioxidant capacities [37]. Unless there is a total ban on BPA, it appears that only the mineralization of BPA for the complete removal of any residual traces of intermediates can be regarded as a prospective viable strategy. Most of the wide variety of approaches proposed in this regard, including bioremediation by microorganisms and oxidative processes, show unsatisfactory performance when targeting the complete mineralization of BPA and derivatives [38–41]. Ozonation could be a better alternative, but the low ozone solubility in water imposes high ozone and energy consumption [42].

Improvements could be brought in the degradation of BPA [43], the distribution of intermediates, and induced toxicity [44] using some metal- and metal oxide-based catalysts such as MnOx/SBA-15. Metals such as iron and nickel were already found to exhibit interesting catalytic activity under both aerobic [45] and anaerobic conditions [46] in the degradation of organic pollutants. Their occurrence in soils and aquatic media is assumed to confer catalytic properties to the host matrix, promoting electron transfer with the organic substrate. Clay-supported metals can improve ozonation by promoting the contribution of adsorption as a compensatory effect for the low solubility of ozone. This approach is regarded as a judicious strategy that takes advantage of the natural ability of soils and aquatic media to self-regenerate, achieving a nature-inspired oxidative degradation process for organic pollutants [47]. Therefore, ozonation catalyzed by metal-loaded clay minerals can be regarded as being quite similar to the oxidative non-biologic processes occurring in most soils and/or clay suspensions in turbid aquatic media exposed to air and solar radiation, even if achieved in an accelerated mode [48,49]. This is the core novelty core of the present work.

Thus, special interest is herein devoted to the ozonation of BPA catalyzed by various montmorillonites exchanged with harmless metal cations (K^+, Ca^{2+}, and Mg^{2+}). Such an approach already demonstrated promising performance in the elimination of a series of organic pollutants [50–54]. Very few works devoted to BPA were focused on the role of clay silanol groups, which appear to promote favorable interactions in both the catalytic process and adsorption [54,55]. Even fewer attempts were made to correlate this role of silanols with the BPA removal rate, intermediate distribution, and toxicity evolution during the process [47,52,53,56–59]. Unless totally mineralized, BPA derivatives can be more toxic than the parent molecule [60]. The partial oxidation of BPA, both in nature and during

water treatment, could have a detrimental effect on biodiversity that warrants further investigation. This is why the present work was undertaken.

For this purpose, the effect of the evolution of intermediate distribution was investigated on the growth of a plant bioindicator, namely *Lemna minor*, which is highly sensitive to ecotoxicity [61]. The latter is a biodiversity representative that grows in most aquatic media potentially exposed to organic pollutants. This work is expected to provide valuable data to predict the degradability of organic pollutants, their intrinsic toxicity, and that of their derivatives according to the exchangeable cation of montmorillonite. As a novelty, attempts are made to correlate the BPA degradation rate and intermediate distribution to the production of reactive oxygen species (ROS) and other toxicity biomarkers for each clay catalyst. The discussion is focused solely on early ozonation, supposedly in the absence of major side reactions of intermediate decomposition.

2. Materials and Methods

2.1. Clay Catalyst Preparation and Characterization

In a first step, sodium-exchanged montmorillonites, denoted as NaMt, were obtained through the purification of an Aldrich bentonite (Sigma-Aldrich, Burlington, MA, USA) with an Si/Al mole ratio of 2.50, a cation exchange capacity (CEC) of ca. 98–100 meq/100 mg, and a specific chemical composition (Table S1) according to a conventional procedure [62]. This allowed removing dense silica phases (mainly quartz and cristaloballite) and other volcanic ashes (mainly illite and mica). Thus, 400 g of bentonite and 50 g of NaCl were introduced into 2 L of distilled water and then heated at 80 °C under vigorous stirring for 7 h. After cooling for 24 h, the clay suspension was repeatedly centrifuged and washed with distilled water until no chloride was detected by the aqueous $AgNO_3$ test. The Na^+-exchanged montmorillonite-rich material (NaMt) was recovered by centrifugation and air-drying at 40 °C overnight. In a second step, various ion-exchanged montmorillonites, denoted as KMt, Mg(II)Mt, Ca(II)Mt, and Fe(II)Mt, were prepared through the ion exchange of NaMt in different aqueous 1 M nitrate metal salt solutions at 70–80 °C under vigorous stirring for 4–5 h. Metal cations such as K^+, Ca^{2+}, and Mg^{2+} are harmless, being present in most soils and aquatic media that act as host environments for organic pollutants. Their selection in this research allowed the simulation of the natural partial degradation of organic pollutants by means of clay-catalyzed BPA ozonation, thereby avoiding additional metal toxicity that may interfere with that of BPA and derivatives. The choice of Na^+ and Fe^{2+} was motivated by (*i*) their omnipresence in nature, (*ii*) the catalytic role of Fe^{2+} in soil and water self-regeneration, and (*iii*) the nutritive properties of Na^+ for many living species.

The resulting clay suspensions were then repeatedly dialyzed in fresh deionized water at room temperature (RT) and finally centrifuged and air-dried overnight at 60 °C. The chemical stability of NaMt at a low pH (1–6) for 0–30 min in aqueous HCl solutions was analyzed through X-ray diffraction (XRD) using a D8 Advance Brucker instrument (Madison, WI, USA, CuKα at 1.54051 Å).

Additional analysis of the clay mineral suspension was achieved through inductively coupled plasma optical emission spectrometry (ICP-OES) in order to assess changes in the chemical composition of the clay minerals upon evolving ion exchange in time with the aqueous BPA solution.

Measurements of the particle size (PS) and zeta potential (ZP) of 40 mg samples of Mt powder, previously dispersed in 20 mL of Nanopure water or an aqueous BPA solution, were performed by means of a Malvern Zetasizer device (Ultra Red Label, Malvern Panalytical, Malvern, UK) at 25 °C and plastic containers (DTS1070, Malvern Instruments Ltd., Worcestershire, UK).

2.2. Adsorption and Ozonation Tests

A 10^{-4} M aqueous solution was prepared by dissolving pure and weakly soluble bisphenol A (BPA) (≥98%) supplied by Sigma-Aldrich (Burlington, MA, USA) in Nanopure water under vigorous stirring for 24 h. Progressive dilutions resulted in solutions with different BPA concentrations, which were previously used to plot calibration curves for the different absorbance bands of BPA. This was achieved through UV-Vis spectrophotometry (UV-Vis) using an Agilent-Cary 60 UV-Vis spectrophotometer (1 cm quartz cell) (Agilent Technologies Canada Inc., Mississauga, ON, Canada). Adsorption attempts were performed at RT and after various contact times with 40 mg adsorbent in 20 mL of BPA solution at their intrinsic pH.

Additional experiments were achieved at various imposed initial pH levels, adjusted by adding a few drops of 0.1 M sodium hydroxide (NaOH) or hydrochloric acid (HCl). This is supposed not to affect the pH evolution or to significantly modify the ionic strength. The pH measurements were achieved by means of an Accumet® model 15 pH meter (Fisher Scientific, Pittsburgh, PA, USA) with ±0.01-unit accuracy after 10–20 s of contact time. The choice of HCl was justified by its capacity to preserve the Mt lattice structure through low Al extraction in more severe conditions [63]. All Mt samples showed sharp 001 XRD lines and a perfectly parallel clay sheet layout without detectable 2-theta value shifts or crystallinity losses (Figure S1). Previous works already provided evidence of the chemical stability of Mt towards acidic media for short contact times [62]. HCl concentrations of 0.05 M and 0.25 M induced only H^+ insertion into the interlayer spacing via cation exchange, with no structure alteration at room temperature, even after 24 h acid attack [64].

Further, ozonation attempts were run for various bubbling times by injecting ozone (600 mg·h^{-1}) generated by an A2Z ozone generator (A2Z Ozone Inc., Louisville, KY, USA) into a 50 mL cylindrical glass reactor containing 20 mL of the same stock solution without and with 40 mg of Mt-based catalyst powder at the intrinsic pH and RT. The dissolved ozone concentration was already found to be limited by its low solubility, with a maximum value of approximately 0.4 mmol/L. The latter can be attained after 10–15 min gas bubbling, regardless of the ozone concentration in the carrier gas or the operating conditions [52].

Here, the supernatant was also centrifuged to obtain a clear and non-turbid mixture for analysis. The process progress in time was qualitatively evaluated by measurements of the relative absorbance $(A/A_0) \times 100\%$ of the supernatant of each ozonation mixture through UV-Vis spectrophotometry (Agilent-Cary 60 instrument, Santa Clara, CA, USA, 1 cm quartz cell). The removal rate of BPA was quantitatively assessed for both the adsorption and ozonation processes with a maximum standard deviation of 0.1% using high-performance liquid chromatography (HPLC) on a Waters Alliance 2695 system and an Agilent C18 column (4.6 mm × 150 mm, 5 µm particle size) coupled to a Waters 2487 diode array detector (HPLC-DAD) at 275 nm. Given the low sample volumes with low BPA concentrations, and since no BPA mineralization was targeted, the HPLC analysis was sufficiently accurate to avoid validation by total organic compound measurements (TOC). Gradient elution was employed with a mobile phase of acetonitrile and Nanopure water at a flow rate of 1.0 mL·min^{-1}. The gradient profile was 30% acetonitrile (0 min), increased to 50% (0–5 min), returned to 30% (5–8 min), and finally raised to 70% by 12 min. The injection volume was 20 µL. The removal rate of BPA was calculated using the equations $(1 - A/A_0) \times 100\%$ for adsorption based on the relative UV-Vis absorbance and $(1 - I/I_0) \times 100\%$ for ozonation using the instant/initial HPLC peak area of the residual BPA concentration (A/A_0) as determined by calibration plots.

2.3. Clay Mineral Dispersion Assessment

The adsorption and ozonation mixtures were also analyzed through measurements of the zeta potential (ZP) and particle size (PS) to evaluate the dispersion of the clay material in the aqueous medium. Such media are supposed to behave similarly to natural aquatic environments, where clay particles are highly polydisperse and anisotropic, exhibiting random particle sizes and shapes that interact with BPA, its derivatives, and oxidizing species. Here, the medium pH varied according to these interactions and exerted a direct effect on the Mt suspension's stability [65,66]. This was achieved after dispersing 40 mg of Mt powder in 20 mL of Nanopure water or adsorption and ozonation mixtures. The supernatant was further filtered through filters with a 45 µm pore size for the determination of the content of the released metal cation. This was achieved through analysis by inductively coupled plasma optical emission spectrometry (ICP-OES) by means of an Agilent Technologies 5100 spectrometer (Santa Clara, CA, USA) operating in an axial configuration and equipped with a concentric quartz nebulizer. The measurements were performed after the previous acid digestion of 2 mL of supernatant in an equal volume of concentrated nitric acid (HNO_3, 70%) at 120 °C for 2 h, cooling, and dilution with Nanopure water until a final acidity of 5% (*v*/*v*) HNO_3. A calibration curve, prepared from certified standard solutions (Sigma-Aldrich) in a 5% HNO_3 matrix, was used for quantification in the range of 0 to 25,000 ng·mL^{-1}. Data acquisition and processing were performed using the dedicated ICP Expert software (version 7.4.2.) [66].

The effect of pH and Mt dispersion in the BPA solution on the adsorption and ozonation efficiency ha an indirect influence on the toxicity of the supernatant. Correlation attempts between Mt dispersion and toxicity are based on the central roles of the pH, dissolved metal cations, and byproducts. For this purpose, 3^3 factorial experiment designs were achieved for NaMt and Fe(II)Mt. The effects of the initial pH, ozonation time, and clay mineral amounts on both adsorption and ozonation and some toxicity biomarkers were examined. Each parameter variation range included three different levels, i.e., upper, central, and minimum limits, based on preliminary experiments and a synthetic analysis of the available data (Table S3). NaMt and Fe(II)Mt were taken as the lower and upper limits for the acid–base properties of montmorillonite, given that their induced pH was found to govern their dispersion in the liquid media and their catalytic properties. Calculations of the model coefficient gave polynomial regression equations that described the main response functions for (*i*) both the adsorption and ozonation and (*ii*) the main biomarkers of *L. minor* based on the initial imposed pH (x1), the adsorption and ozonation times (x2), and the clay mineral concentration (x3) (Tables S7 and S8). These mathematical models involve not only the individual effects of the process variables but also their interactions on the different response functions investigated.

2.4. Toxicity Tests on Lemna minor

Lemna minor was cultivated in a standardized SIS nutrient medium (Table S2), adjusted to pH 6.5 ± 0.2, and autoclaved. Plants were grown under controlled conditions: a 16/8 h light/dark cycle (100 ± 10 µmol photons m^{-2} s^{-1}), 24 ± 2 °C, and 60 ± 5% relative humidity. To assess toxicity, BPA solutions (0.001–10 mg·L^{-1} in Nanopure water)—both before and after adsorption or ozonation—were tested. The testing process was conducted in accordance with the requirements established by the Organization for Economic Cooperation and Development (2006) [61]. All tests were reported to the control sample, which consisted of a SIS medium containing *Lemna minor* without ozonation. The blank sample depends on the experiment and could be a control sample without BPA or without the clay mineral, as defined in the captions of each figure.

For each replicate, 5 mL of test filtrate was combined with 20 mL of SIS medium and three triple-fronded plants in a 50 mL Erlenmeyer flask; the control contained only plants in 25 mL of SIS medium. After 7 days of exposure, the growth inhibition was estimated from various biomarkers (μ), such as the frond number, fresh weight, chlorophyll content, and ROS production with respect to that of the control, using the relationship

$$\% \text{ inhibition} = 100 \times \left(1 - \frac{\mu_{\text{sample}}}{\mu_{\text{control}}}\right) \quad (1)$$

The intracellular ROS levels were measured fluorometrically in whole plant tissue using the CellROX® Green reagent (Thermo Fisher Scientific, Waltham, MA, USA). After the 7-day exposure period, plants were gently blotted dry and incubated for 30 min at 25 °C in the dark with 5 μM CellROX Green (excitation/emission maxima: 485/520 nm). Subsequently, the plants were rinsed with phosphate-buffered saline (PBS) for 10 min at room temperature to remove excess probe. Relative fluorescence was measured at an emission wavelength of 520 nm (excitation: 485 nm; gain: 200) using the same microplate reader. The measured ROS production was normalized per unit of biomass (fresh weight).

Chlorophyll (Chl) was extracted from *Lemna minor* fronds by mechanical homogenization in 5 mL of 95% (*v*/*v*) ethanol at room temperature. The resulting homogenate was centrifuged, and the absorbance of the supernatant was measured at 665 nm and 648 nm using a microplate reader (Infinite M200®, Tecan, Switzerland). The concentrations of chlorophyll *a* and chlorophyll *b* (μg·mL^{-1}) were calculated according to Lichtenthaler's equations (1987) [67]:

$$\text{Chl } a = 13.36A_{665} - 5.19A_{648} \quad (2)$$

$$\text{Chl } b = 27.43A_{648} - 8.12A_{665} \quad (3)$$

One typically expects a detrimental effect of a low pH on *L. minor* below that of the SIS media. Like ozonized mixtures, all naturally oxidized waters containing organic molecules released in/on soils and/or aquatic media have a low pH and a detrimental effect on biodiversity. This is why the present work was undertaken. In this work, no pH adjustments at the SIS level are recommended, because the addition of acids or bases (diluted HCl or NaOH) causes the unavoidable modification of the ionic force and possible modification of the targeted toxicity induced by BPA and derivatives.

3. Results and Discussion

3.1. pH Effect on BPA Adsorption

The 195–205, 225 nm, and 275 nm bands in the UV-Vis spectrum of the supernatant showed noticeable intensity decreases during the first five minutes of bisphenol A (BPA) adsorption (Figures S2 and S3). These bands involve mainly π-π* and *n*-π* transitions of the aromatic ring, being accurate indicators of BPA depletion by adsorption. The more pronounced intensity decreases registered for NaMt and, to a lesser extent, MgMt and bentonite account for the higher adsorption efficiency as compared to the other Mt-based adsorbents and must be related to the acid–base properties of their exchangeable cations. Among these, Na^+ and Fe^{2+} can be regarded as reasonable limits for investigating the acid–base properties of ion-exchanged montmorillonites in organically polluted waters, which are mostly acidic media, often barely reaching pH 6. No detectable alteration of the Mt structure and crystallinity was noticed within the pH range of 1–6 for contact times below 30 min. This justified the choice of the central value of 15 min for the pH in the further modeling–optimization step.

Imposing various initial pHs in this range on BPA adsorption on NaMt and Fe(II)Mt revealed an almost linear increase in the final pH from 1 to 3 (Figure 1). This is due to

an increase in the Na^+/H^+ and Fe^{2+}/H^+ concentration ratios in their respective liquid media due to the dissolution of Fe^{2+} from the dispersed $Fe(OH)_2$ suspension at pH 2, followed by consecutive capture by progressively deprotonated BPA molecules and silanols. The shading effects of the imposed acidity and simultaneous proton release upon the progressive conversion of the -Si-OH_2^+ groups into neutral SiOH should fade, leading to total disappearance, when approaching pH 3–4. At this level, close to the pH-zero charge (pH_{ZC}) of many types of silicas and aluminosilicates [68–71], an increase in attenuation in the final pH occurred up to the intrinsic pH imposed by Na^+ and Fe^{2+} in their corresponding Mt suspensions.

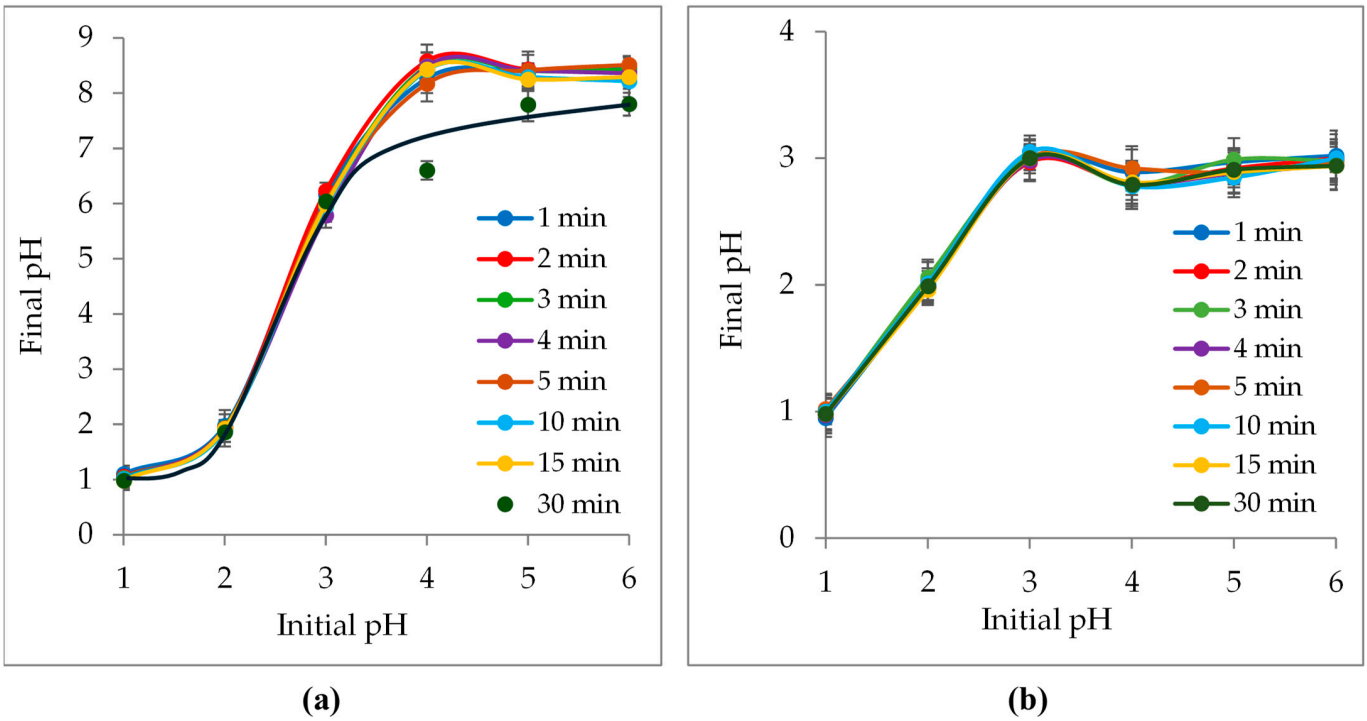

Figure 1. Initial pH effect on the final pH of the aqueous media during BPA adsorption on NaMt (**a**) and Fe(II)Mt (**b**). T: 25 °C. Volume: 20 mL. BPA concentration: 10^{-4} M. Mt amount: 40 mg (2 g·L^{-1}). The initial pH is a pH initially imposed by adjustments by the addition of adequate amounts of 0.1 M aqueous HCl or NaOH solutions. The initial pH was measured after 20–30 s of contact time after adding the clay adsorbent to the BPA solution.

In this pH range, no marked effect of the pH was observed given the almost similar evolutions of the UV-Vis spectra of the supernatants of NaMt and Fe(II)Mt suspensions (Figures S4 and S5). Nonetheless, HPLC-DAD revealed major fluctuations, with a barely detectable decay in the retention rate depending on the contact time for NaMt and a significantly more visible one, from 80–84% down to 45–60%, for Fe(II)Mt (Figures S6 and S7). A plausible explanation resides in the almost total lack of BPA/Mt electrostatic interaction. Indeed, with pKa1 and pKa2 around 9.59 and 10.2, respectively [72], BPA molecules should be almost totally neutral below pH 3 and in a 99.9999% proportion at pH 4.

This ought to restrict BPA adsorption mainly to hydrophobic [methyl:siloxy] interactions and hydrophilic [phenol–phenol] intermolecular H-bridges (Scheme 1), as already reported [54]. In this pH range, the adsorbed neutral BPA molecules should contribute to Mt lamella cementation, leading to particle aggregation via [Mt:BPA:BPA:Mt] sandwiching interactions (Scheme 1).

Continuous pH increases from 4 to 6 induced no modification in the final pH, which stabilized at 8.3–8.4 after 15 min adsorption time on NaMt and 6.6–7.8 for longer contact times (Figure 1a), but at only 2.8–3.3 for Fe(II)Mt due to the Bronsted acidity of Fe^{2+} cations

(Figure 1b). This result provides clear evidence that the effect of the exchangeable cation is strongly dependent on the pH. Conversely, this effect is expected to induce an intrinsic pH in the Mt suspension and to govern the interaction between the cation, BPA molecules, and/or Mt surface.

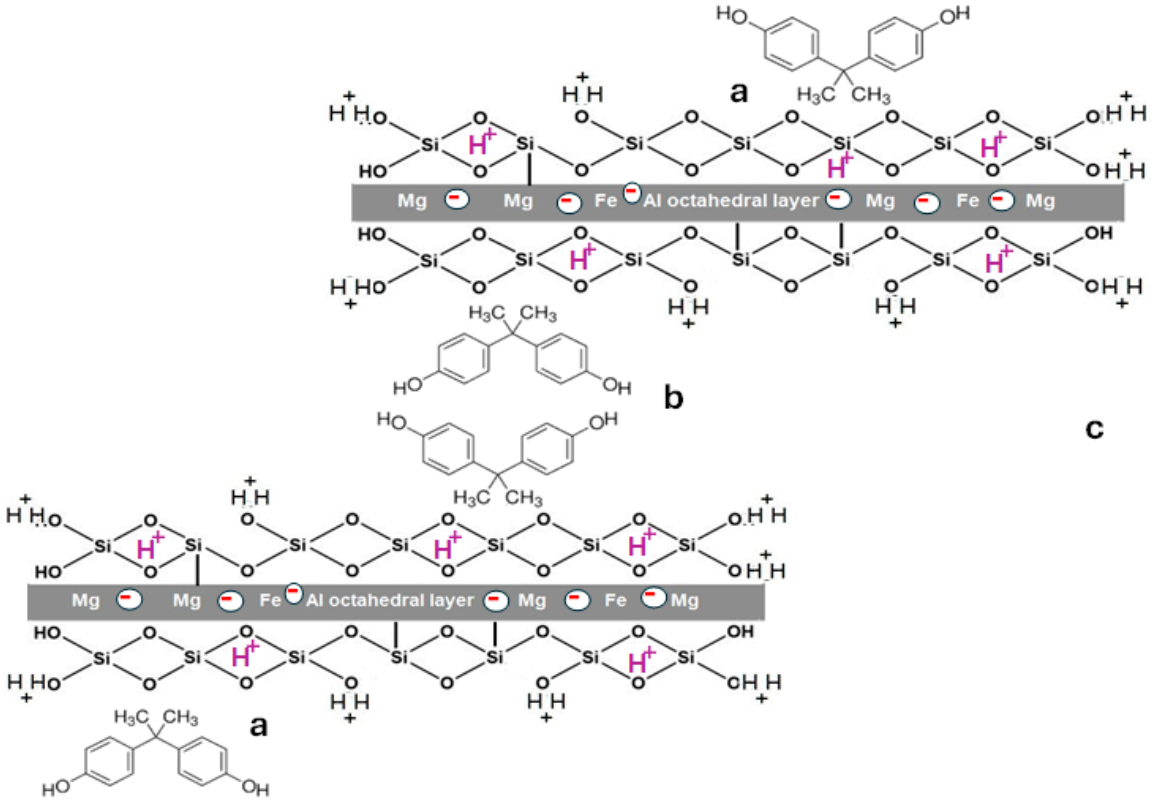

Scheme 1. Illustration of the cementing [methyl:siloxy] interactions (a) and [phenol:phenol] intermolecular H-bridges (b) in aqueous media containing H^+ excess and Na^+ or Fe^{2+} cations at a pH below the pH_{ZC} (c).

3.2. Cation Transfer During Adsorption

The progressive conversion of $SiOH_2^+$ groups into neutral SiOH induces a depletion of the repulsive positive charges when approaching the pH_{ZC}, which explains the noticeable ZP decrease (Figure 2). This pH threshold is expected to trigger SiOH deprotonation into SiO^- groups, unavoidably leading to (*i*) the rise of repulsive negative charges on both BPA molecules and the Mt surface and Mt lamella dispersion through exfoliation and delamination; (*ii*) an enhancement in the hydrophilic character; (*iii*) BPA slight desorption via competitive interaction with water molecules; (*iv*) cation capture, probably by both BPA and Mt surfaces. In montmorillonite, within the investigated pH range of 1–6, the negative charges mainly originate from ≡S-O-based associations with Si, H, and Al or Mg atoms. The latter exhibit various pKa values, including 5.3 (≡$Si(OH)_2Mg$), 5.9 (≡$Si(OH)_2Al$), and 6.3–10.41 for many types of (≡Si(OH)) groups for various spatial conformations and surrounding atoms. Given their relatively high pKa values of 10.1 (≡$Al(OH_2)(OH)$) and 13.2, the (≡Al(OH)Al sites on the edge structure should display only a minor contribution to the negative surface charge [73]. The presence of Mg^{2+} appears to increase the pKa values of neighboring areas [73].

The improvement in the hydrophilic character is well illustrated by the hypsochromic shift of the 195–205 nm band, which accounts for *n*-π* interactions with water molecules. At pH 6, the hypsochromic shift reached ca. 15 nm (from 210 nm to 195 nm) after 30 min, being more pronounced at higher pH values (Figures S4 and S5). This enhancement in BPA's

interaction with water molecules as the pH increases must also involve BPA deprotonation, which contributes to cation capture through ion exchange.

The rise of surface negative charges is expected to shade and mitigate the decrease in ZP and to enhance the cation capture from the liquid media (Figure 3). This is well illustrated by the visible decrease in the Na^+ concentration in the adsorption medium, reaching a plateau at pH 3. Its globally lower concentration in the aqueous media for 30 min of BPA adsorption on NaMt agrees with the lower plateau of the final pH (Figure 1a).

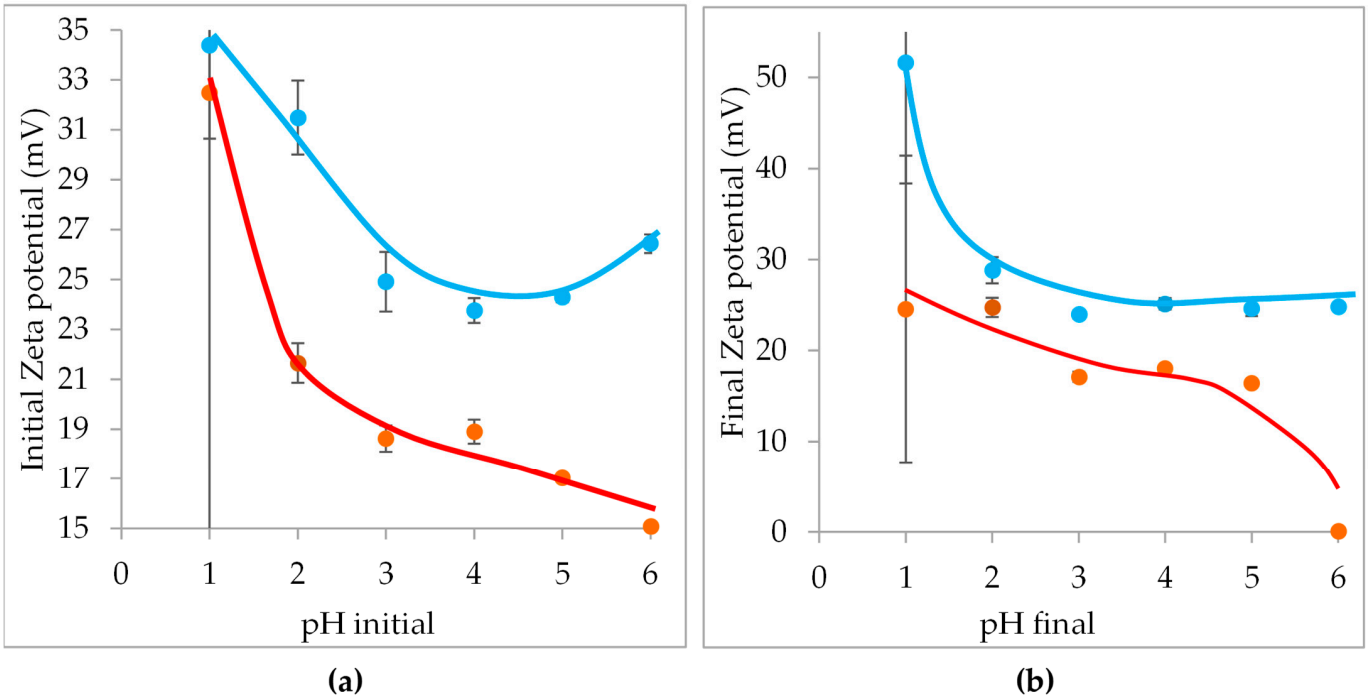

Figure 2. Zeta potential versus the initial (**a**) and final pH (**b**) for BPA adsorption in the presence of NaMt (red) and Fe(II)Mt (blue). T: 25 °C. Sample volume: 20 mL. BPA initial concentration: 10^{-4} M. Mt amount: 40 mg (2 g·L^{-1}). The initial pH was measured after 20–30 s of contact time after Mt addition to the BPA solution. The initial zeta potential was measured after 5 min of contact time after Mt addition to the BPA solution. The final ZP was determined after 30 min of adsorption.

For Fe(II)Mt, the plateau at pH 2.8–3.3 corresponds to the lowest Fe^{2+} concentrations of around 1 ppm in the liquid media and does not seem to be influenced by the adsorption time, unlike for NaMt (Figure 3b). Thus, BPA capture on ion-exchanged montmorillonite appears to take place with simultaneous pH-dependent cation exchange between the solid surface, deprotonated BPA molecules, and impregnating media. These cation transfers may influence the very adsorption of BPA and Mt's behavior in the aqueous media.

Thus, since an increasing initial pH favors cation capture from the liquid media during adsorption (Figures 2 and 3), the reverse phenomenon should occur during ozonation regardless of the cation. The clay mineral cations are substituted by protons provided by the produced acidic species, which in turn should capture the released cation. Fe^{2+} precipitation, if any, is not supposed to take place above pH 2 or when the cation is captured by ion exchange or chelation.

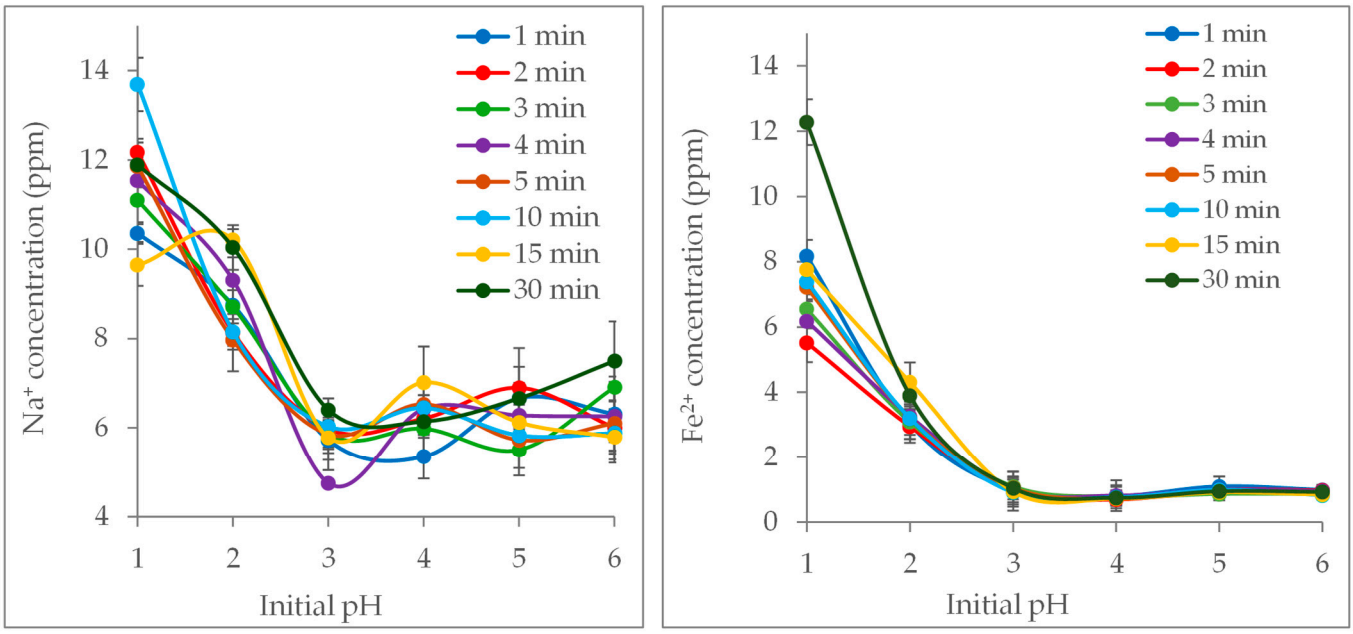

(**a**) (**b**)

Figure 3. Initial pH effect on the cation concentrations in the supernatant of the aqueous media after BPA adsorption on NaMt (**a**) and Fe(II)Mt (**b**) in Nanopure water as assessed by ICP-OES. T: 25 °C. Sample volume: 20 mL. BPA initial concentration: 10^{-4} M. Mt amount: 40 mg (2 g·L^{-1}). The initial pH was measured after 20–30 s of contact time after adding Mt to the BPA solution.

3.3. Effects of pH on Clay Dispersion

An imposed pH increase between 1 and 6 leads to weak but sufficient silanol deprotonation that promotes clay dispersion and the exposure of preponderant protonated silanols to the bulk solution. The consecutive enhancement in the hydrophilic character and in the density of the negative charges induced Mt lamella dispersion through delamination and exfoliation, as supported by the marked decrease in particle size (Figure 4). Such a phenomenon was already reported for acid-activated bentonites, where the clay dispersion was found to be governed by the hydrophilic–hydrophobic ratio of the surface [54]. The latter is strongly dependent on the pH of the aqueous medium. This phenomenon appears to reduce the contribution of the [Mt:BPA:Mt] cementing interaction and to determine the orientation of the hydrophobic/hydrophilic side of the BPA molecule towards the bulk solution (Scheme 2).

The mere presence of BPA molecules appears to reverse the surface hydrophobic characteristic, thereby promoting cation capture by deprotonated BPA hydroxyl groups and silanols. This ought to maintain the methyl groups of the adsorbed BPA towards the siloxy islands on the Mt surface and to expose accessible OH groups and deprotonated counterparts towards the bulk solution, which is assumed to promote and enhance particle dispersion. The consecutive decrease in the particle size is known to improve the accessible contact surface, which should favor clay-catalyzed ozonation.

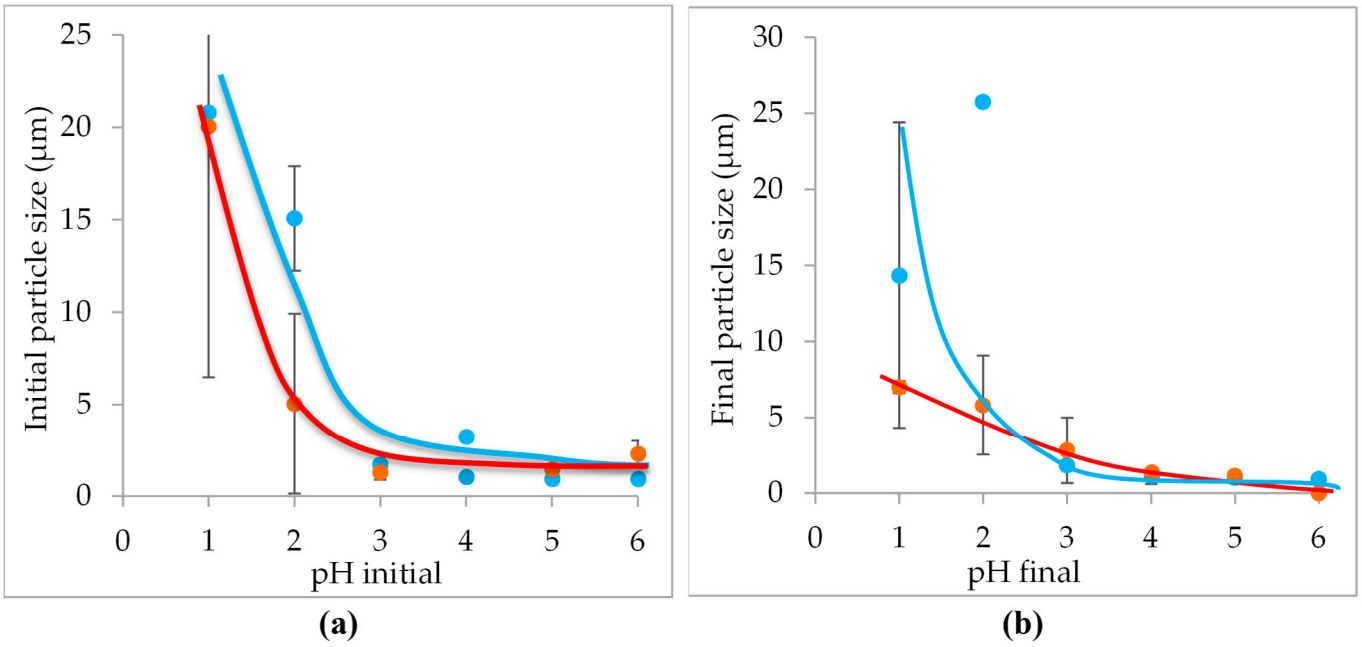

Figure 4. Correlations of the particle size with the initial (**a**) and final pH (**b**) for BPA adsorption in the presence of NaMt (red) and Fe(II)Mt (blue). T: 25 °C. Sample volume: 20 mL. BPA initial concentration: 10^{-4} M. Mt amount: 40 mg (2 g·L^{-1}). The initial pH was measured after 20–30 s of contact time after adding the clay adsorbent to the BPA solution. The final pH was determined after 30 min of the adsorption process.

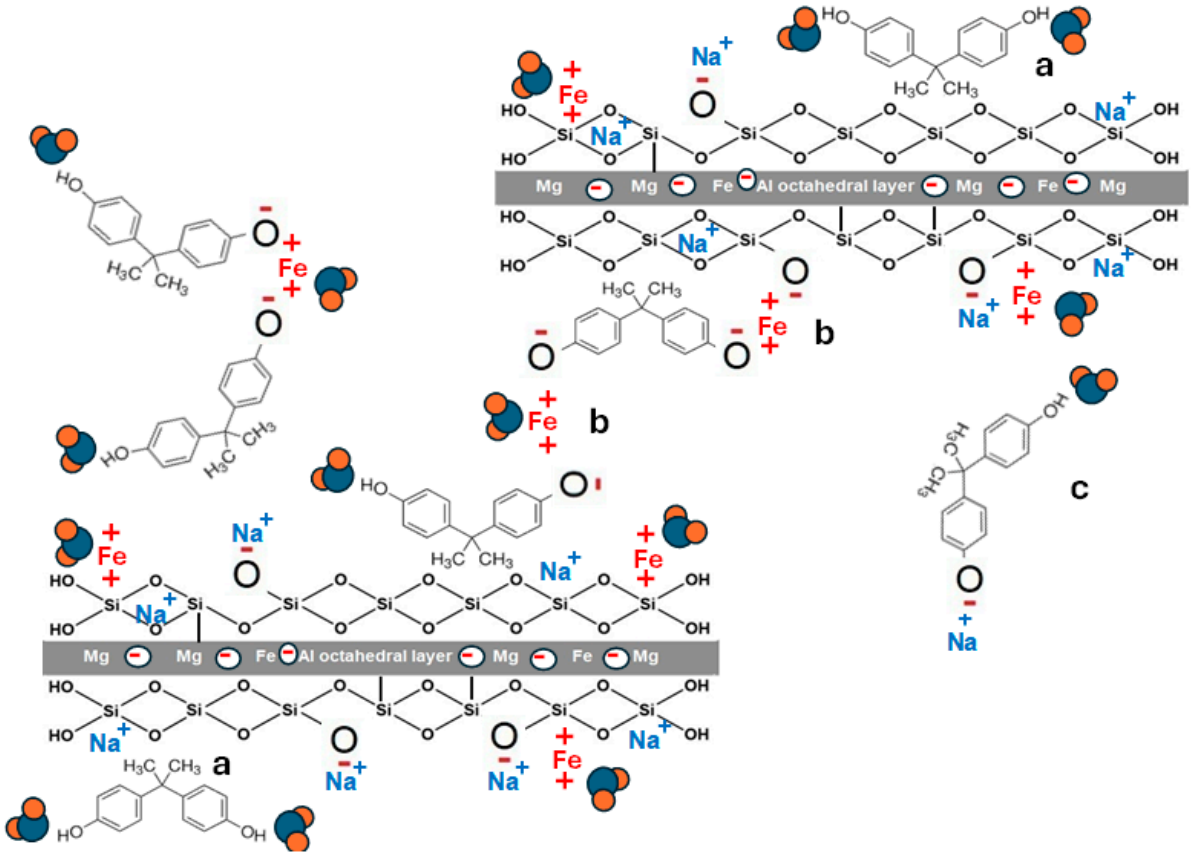

Scheme 2. Schematic illustration of cation exchange by both deprotonated exchangeable sites, silanols, and both adsorbed and free BPA at a pH above the pH_{ZC}: (a) hydrophobic [methyl:siloxy] interactions; (b) [BPA-O-:Fe^{2+}:-O-BPA], [BPA-O-:Fe^{2+}:-O-Mt], and [Mt-O-:Fe^{2+}:-O-Mt] bridges; (c) BP-containing media with fewer H^+ and Na^+ or Fe^{2+} cations.

3.4. Correlation Between Adsorption and Ozonation

During ozonation, a global intensity increase for the 220–245 nm UV band was observed during the first 10 min (Figures S8 and S9). This was attributed to $\pi \rightarrow \pi^*$ and $n \rightarrow \pi^*$ electronic transitions, which indicate the formation of carboxylic acids [74]. The specific $\pi \rightarrow \pi^*$ transition of the carbonyl group involving transitions from a π bonding orbital to a π^* antibonding orbital can be observed at shorter wavelengths of around 190 nm. The $n \rightarrow \pi^*$ transition results from the transition of a non-bonding electron on the oxygen towards an antibonding π orbital. Possible n $\rightarrow$ σ^* transitions may also involve electron transfer from a non-bonding (n) orbital to an antibonding sigma (σ^*) in this high-energy region when saturated alcohol molecules with lone pairs of non-bonding electrons are produced, more particularly after phenyl ring cleavage. Such a process requires severe oxidation conditions, often involving radicals, which, however, are expected to have only a minor contribution in the acidic media of clay-catalyzed ozonation as compared to BPA photocatalytic degradation [75,76]. In the meantime, the 275 nm band showed a stronger increase in intensity compared to the 225 nm band, detectable from 10 to 30 min. This band was attributed to the lower-energy $n \rightarrow \pi^*$ transition of non-bonding electrons from oxygen atoms of hydroxyls on the aromatic ring to antibonding π^* orbitals [77,78]. This suggests chemical modifications of the phenolic ring. Here, hydroxylation is probably the main modification in this regard. Ring cleavage and/or hydroxylation were found to be the main reactions that generate catechol, orthoquinone, muconic acid, benzoquinone, and 2-(4-hydroxyphenyl)-propan-2-ol [79].

Most BPA oxidation intermediates absorb in this spectral region. In addition, all derivatives bearing hydroxyls should interact with water molecules, inducing electronic transitions depicted by a broad shoulder in the region of 300–400 nm and charge transfer transitions from water to the OH group as illustrated by a high-intensity band around 230 nm. This unavoidably shades the depletion in time of the very UV bands of the parent molecule [59]. This is a major limitation of UV-Vis spectrophotometry that restricts its use to only a qualitative assessment of the ozonation progress but allows affording a quite reliable evolution in time of BPA removal through adsorption (Figure S10). The quantitative evaluation of BPA conversion during ozonation using high-performance liquid chromatography enabled an accurate assessment of BPA depletion during both adsorption and ozonation (Figure S11). As a common feature, ozonation gave a higher BPA removal rate as compared to adsorption alone for all clay minerals investigated herein (Figure 5). This suggests a contribution to BPA capture by the clay surface prior to its oxidative conversion. The role of adsorption in the catalytic ozonation process was evidenced by proportional increases in the BPA removal rate for both processes, as well as an improvement leading to total BPA disappearance after approximately 1 min of NaMt-catalyzed ozonation and about 15 min with the other clay catalysts. NaMt and, to a lesser extent, bentonite showed the highest retention rates of 100% after 5 min contact time and ca. 85% after 30 min contact time, respectively.

Equilibrium was attained after 5–10 min contact time, and maximum adsorption capacities of 72.26%, 87%, 66.96%, and 55.86% were registered for CaMt, bentonite, KMt, and Fe(II)Mt, respectively, after 30 min contact time. Fe(II)Mt was already found to exhibit very similar catalytic performance, including the adsorption contribution [59].

This complete BPA degradation took place without total mineralization, which, however, seems to be difficult to achieve even in the presence of hydroxyl radicals at a higher pH [80]. For most bisphenols, oxidation generates catechol and derivatives in the first step, followed by the formation of ortho-quinone intermediates, ring cleavage products, and phenolic derivatives [76,81–83]. Derivatives such as catechol, acetone, hydroquinone, formaldehyde, acetic acid, formic acid, maleic acid, oxalic acid, and others exhibit higher chemical

stability with respect to ozone than their less oxidized counterparts, which explains their persistence even after 30 min of ozonation and thorough BPA disappearance [84,85].

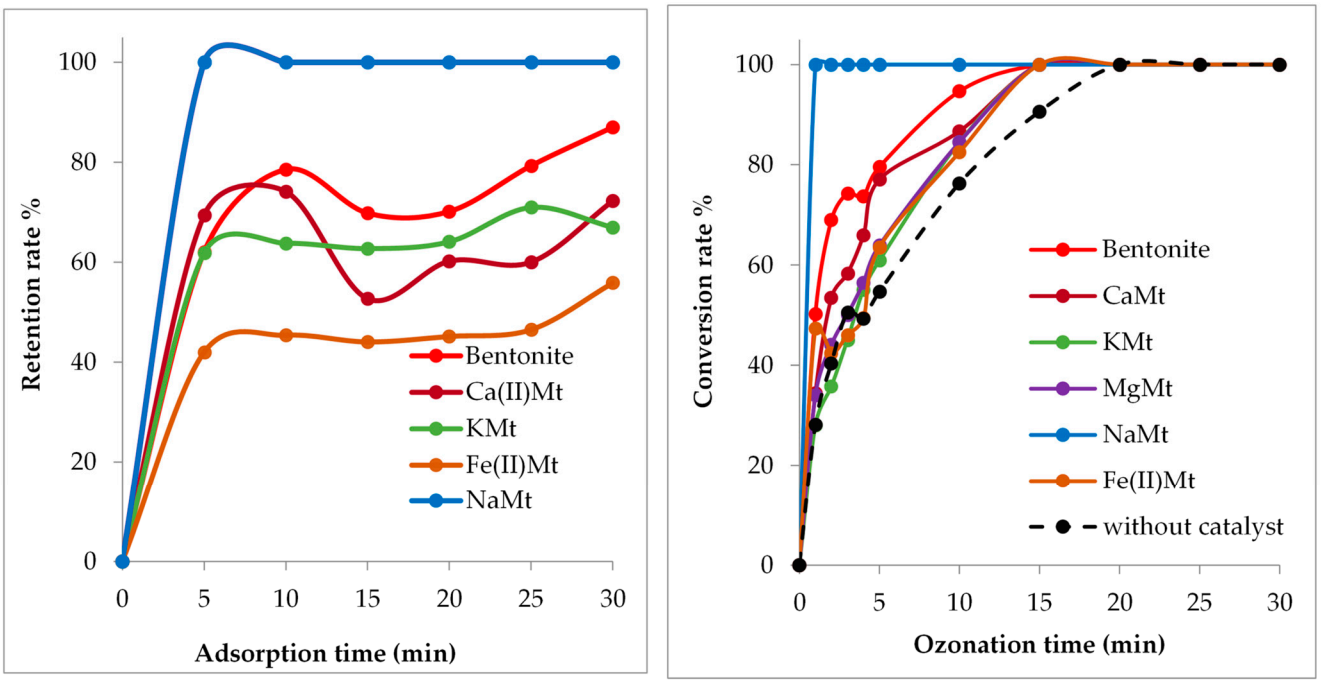

(**a**) (**b**)

Figure 5. Removal rates of BPA by adsorption (**a**) and ozonation (**b**) as assessed through HPLC-DAD. V = 20 mL of Nanopure water or 10^{-4} M BPA solution at RT; ozone throughput = 600 mg·h^{-1}; Mt amount = 40 mg (2 g·L^{-1}). The BPA residual concentration was determined in the supernatants of the Mt suspensions at their initial intrinsic pH. The BPA peak was monitored at a retention time of 7.1 min using a 30/70 (*v*/*v*) water/acetonitrile gradient. The HPLC-DAD peak of BPA was monitored at a retention time of 7.1 min using a 30/70 (*v*/*v*) water/acetonitrile gradient.

3.5. pH Evolution During Adsorption and Ozonation

For NaMt, BPA adsorption induced a slight decrease in pH from the starting intrinsic pH of the BPA-containing suspensions of NaMt and bentonite (8.18) down to a plateau of 7.40–7.16 after 15–20 min (Figure 6a). All other Mt suspensions showed a visible pH from their respective intrinsic pH up to constant levels at pH 7.04 for MgMt, 6.78 for CaMt, 6.11–5.73 for KMt, and 3.6 for Fe(II)Mt after only 5 min during BPA adsorption. This sequence corresponds to the increasing Lewis acidity and polarizing power of the investigated exchangeable cations, which determine its Bronsted acidity in aqueous media [86,87]. This result suggests cation removal from the aqueous media, presumably by ion exchange on deprotonated silanols and BPA molecules, as well as via chelation by its hydroxyl groups, in agreement with the previous statements.

In contrast, a rapid pH decrease was observed during the first 1–10 min of ozonation (Figure 6b). This is most likely due to the formation of acidic by-products. Additionally, this trend was accompanied by a noticeable reduction in the rate of pH decrease, likely due to increasing buffering effects. Such changes may be caused by the unavoidable release of Fe^{2+} cations during ion exchange on the clay surface, which can be captured not only by deprotonated BPA molecules but also by carboxyl groups from acidic species produced by ozonation. This result is significant because it shows that BPA adsorption causes specific pH changes that depend on the exchangeable cation, which in turn influences the ozonation process.

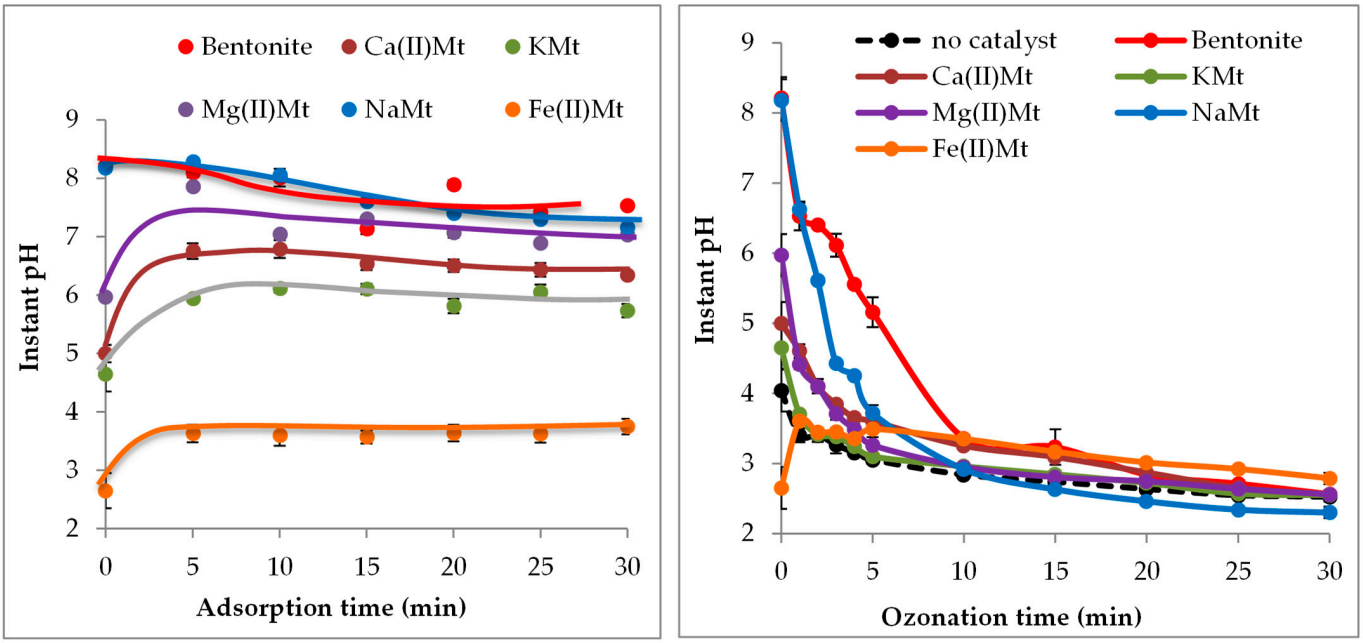

(**a**) (**b**)

Figure 6. pH evolution during adsorption (**a**) and ozonation (**b**) in the presence of clay adsorbents/catalysts at the intrinsic pH and RT. O_3 throughput: 600 mg·h^{-1}. Sample volume: 20 mL. BPA initial concentration: 10^{-4} M. Clay mineral amount: 40 mg (2 g·L^{-1}).

3.6. Supernatant Toxicity After Adsorption/Ozonation

An integrated approach was adopted to assess the simulated effects and interactions of the parameters that govern adsorption and ozonation and the influences of both processes on the toxicity of their BPA mixtures towards *Lemna minor*. BPA is a synthetic organic compound that acts as an exobiotic chemical substance, exhibiting intrinsic toxicity towards the growth and metabolism of living organisms, even before its degradation. The toxicity of various adsorption or ozonation mixtures was assessed after 7 days of contact with *L. minor*-containing SIS media. An initial analysis of the results revealed a visible increase in the initial pH of the *L. minor*-containing SIS media (pH 6.5) immediately after contact with the adsorption mixtures in the presence of most Mt adsorption (Figure S12a). This can be explained in terms of cation consumption from the liquid media as nutrients by the plant. The more significant pH increase registered with bentonite must be due to massive release by basic alkali and alkaline earth cations upon ion exchange at this starting pH level of 6.5. The fluctuations in the final pH as measured after 7 days of exposure of *L. minor* to the adsorption mixtures suggest the occurrence of complex cation transfers from/to the clay mineral, liquid media BPA molecules, and plant specimens (Figure S12b). After ca. 10 min exposure, the pH almost stabilized at ca. 6.8 to 7.25 according to the clay mineral, presumably due to the progressive depletion of BPA by adsorption. This result is of great importance because it clearly demonstrates the intrinsic toxicity of BPA, whose depletion leads to a global slight improvement in the proportions of plant fronds and specimens (Figure S13) and the fresh weight (Figure 7a).

In contrast, ozonation mixtures induced a sharp and rapid pH drop after approximately 10 min, a so-called "induction period", down to 2.75–3.4 after 30 min of contact time (Figure S14). A similar pH decrease was observed for the final pH, but this was delayed to 20–25 min. This can be explained by the formation of acidic BPA derivatives. This is likely due to an initial oxidative stress of the investigated vegetal bioindicator. A first analysis of the data obtained revealed significant and progressive decays in the proportions of plant fronds and specimens and the fresh weight (Figure 7b) as reported to the initial non-altered

SIS media, reaching 28–54%, 28–48%, and 25–56%, respectively, after 7 days of exposure of *Lemna minor* to the ozonation mixtures (Figure S15).

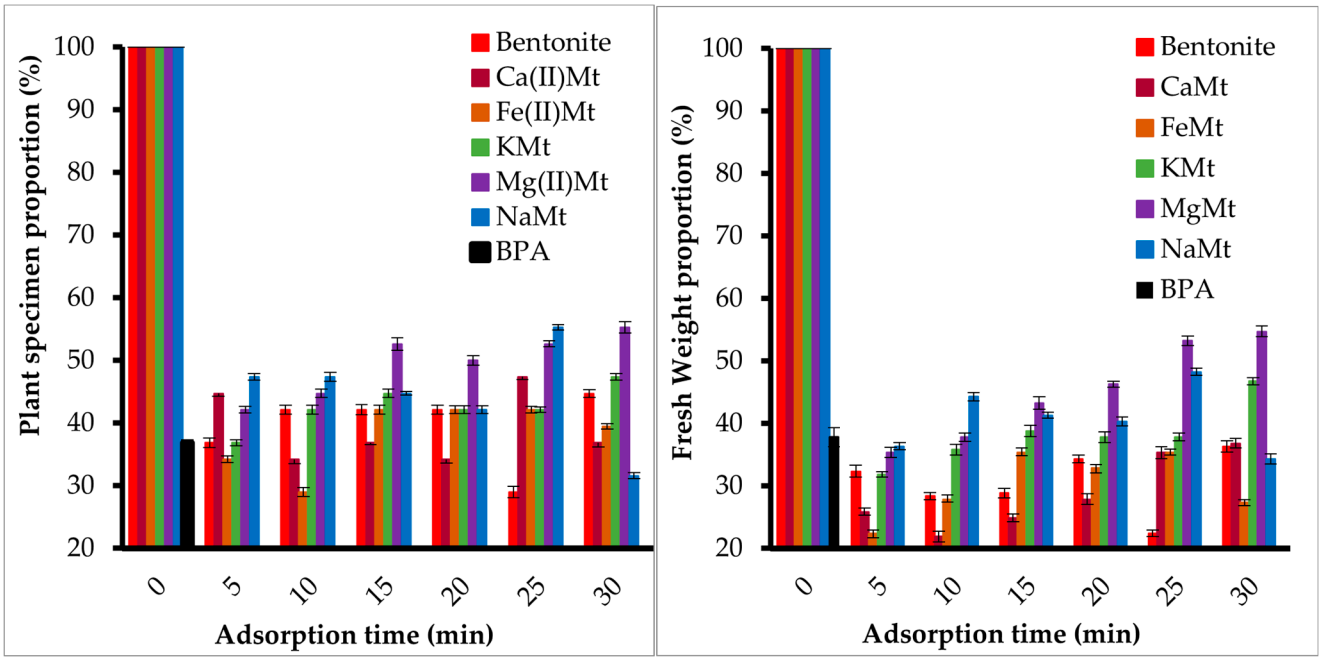

Figure 7. Effects of the adsorption mixture on the proportions of plant specimens (**a**) and the fresh weight of *Lemna minor* (**b**) as reported to the blank sample (control). The results are expressed as percentages relative to the control sample (BPA-free SIS medium). These data account for the means of triplicate measurements after plant exposure for 7 days, including the control sample and the supernatant of the adsorption mixture.

This detrimental effect of the ozonation mixtures on the normal growth of the plant involves (*i*) the rise in acidic and potentially toxic derivatives and (*ii*) changes in the cation distribution of the SIS media through ion exchange by the clay surface and deprotonated BPA molecules, as well as chelation by neutral BPA molecules. The weakest impacts were registered for MgMt and NaMt and, to a lesser extent, CaMt, which are known to be essential nutrients for *L. minor*. The most pronounced depletion was obtained for Fe(II)Mt, bentonite, and KMt. A slight revival of these three biomarkers was noticed after 15 min adsorption time, but they remained, by far, very low with respect to the starting unaltered SIS media.

3.7. Production of Reactive Oxygen Species

As expected, fluctuations were also observed in the production of reactive oxygen species (ROS) after the contact of the *L. minor*-containing SIS media with the adsorption and ozonation supernatants. Higher ROS levels were noticed for short times not exceeding 5 min of BPA adsorption on Fe(II)Mt, bentonite, and NaMt (Figure 8a) and for the ozonation of BPA alone or in the presence of MgMt, NaMt, and Fe(II)Mt (Figure 8b). Except for MgMt, and a few fluctuations for Fe(II)Mt, the global and apparently uniform decrease in the ROS level during adsorption must arise from the progressive BPA removal and related toxicity decay.

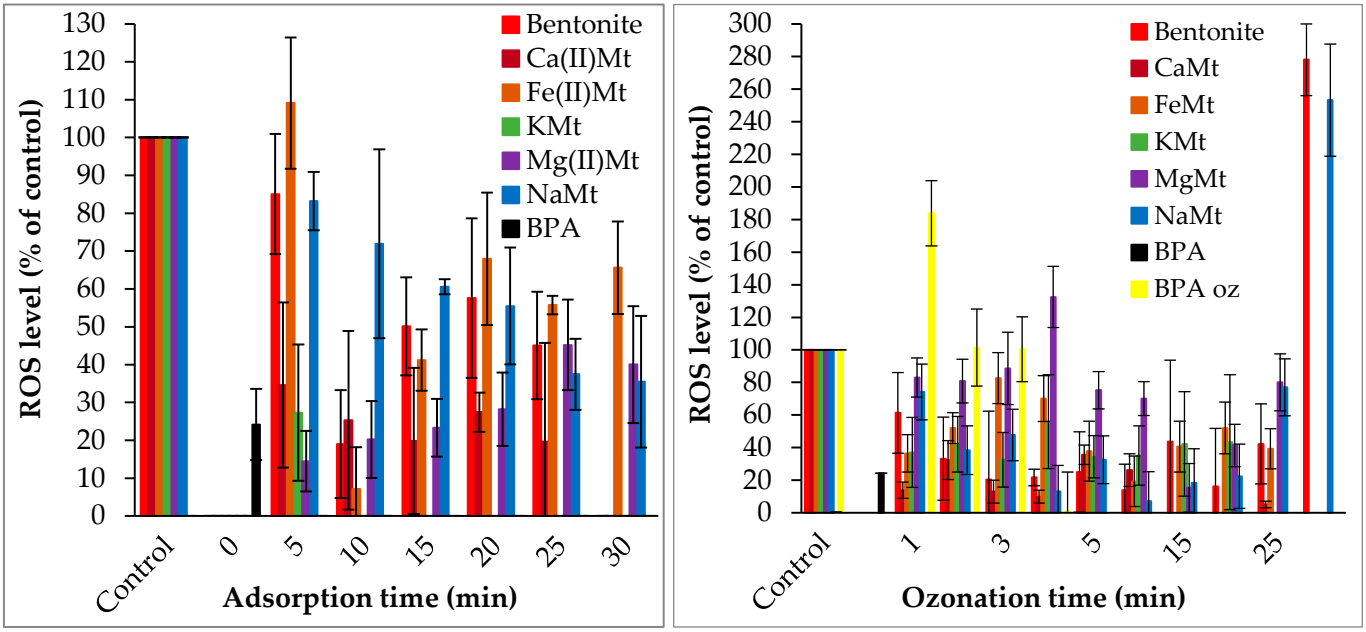

(**a**) (**b**)

Figure 8. ROS level variation during adsorption (**a**) and ozonation (**b**). These data account for average triplicate measurements after plant exposure for 7 days, including the control sample (*Lemna minor* in SIS medium without BPA) and the supernatants of the adsorption or ozonation mixtures. T: 25 °C. O_3 throughput: 600 mg·h^{-1}. Sample volume: 20 mL. BPA initial concentration: 10^{-4} M. Clay mineral amount: 40 mg (2 g·L^{-1}).

ROS levels higher than that of the control sample are due to the occurrence of a hormesis phenomenon, as a *L. minor* response to an oxidative stress caused by reaction mixtures after the first 4–5 min of ozonation. The latter could be induced by (*i*) the presence of acidic and/or toxic species and (*ii*) changes in cation distribution in the SIS medium. ROS fluctuations during Mt-catalyzed ozonation appear to vary according to the exchangeable cation of montmorillonite, which should govern the distribution of acidic and/or toxic species and the chemical composition of the SIS medium. An ROS level revival was also observed for prolonged periods of adsorption and ozonation, namely 20–30 min adsorption and 30 min ozonation, in the presence of bentonite or NaMt. This agrees with the previous recovery of the plant growth registered for adsorption (Figure 7a) and ozonation (Figure 7b). Thus, it clearly appears that BPA degradation under aerobic conditions reduces the toxicity but exerts an unavoidable overall impact on the environment before achieving thorough mineralization into carbon dioxide and various oxides.

This induced toxicity towards *L. minor* was reflected by an increase in the chlorophyll *a*/*b* ratio during adsorption, which was even more pronounced during ozonation, reflecting a detrimental effect on the photosynthetic efficiency of *Lemna minor* (Figure 9). This phenomenon arises from a global increase in the proportion of Chl *a* at the expense of its counterpart Chl *b*, with visible ROS fluctuations according to the exchangeable cation during both adsorption and ozonation, as previously stated. However, the global pigment content was found to decrease only during ozonation, likely due to an irreversible alteration in the photosynthetic system (Figure S16).

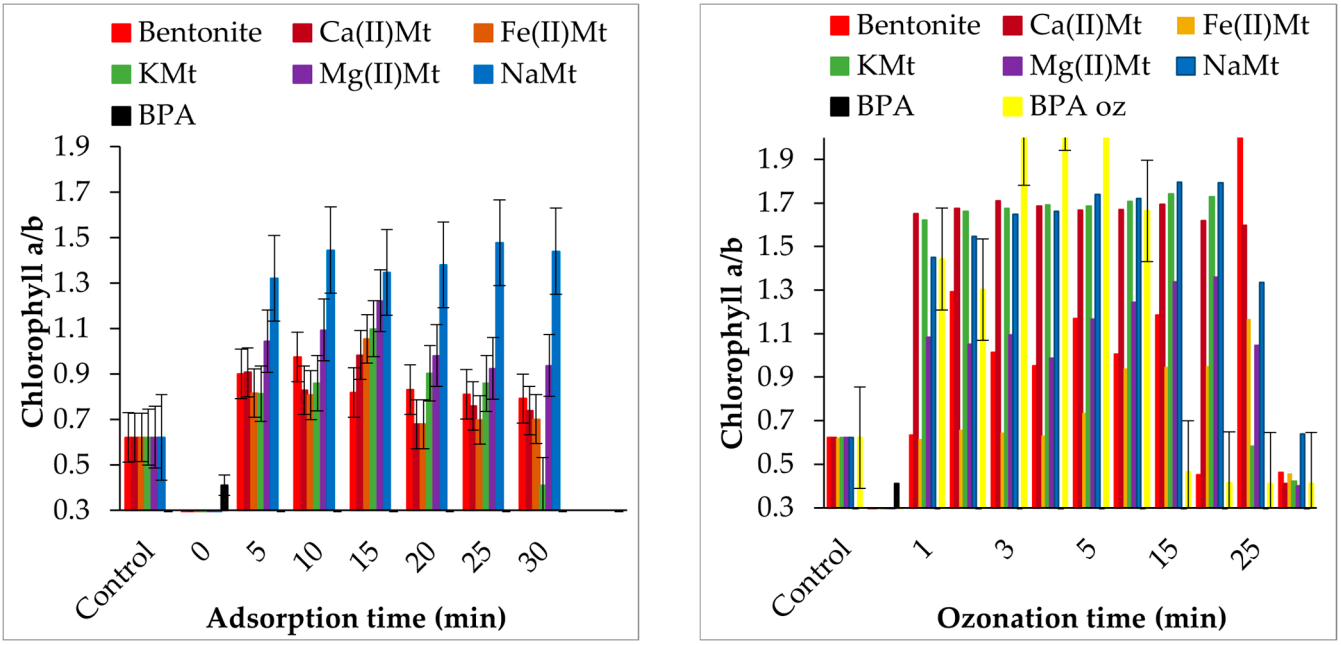

Figure 9. Evolution of the chlorophyll *a*/*b* ratio during adsorption (**a**) and ozonation (**b**). These data account for an average of triplicate measurements after plant exposure for 7 days, including the control sample (*Lemna minor* in SIS medium without ozonation). T: 25 °C. O_3 throughput: 600 mg·h^{-1}. Sample volume: 20 mL. BPA initial concentration: 10^{-4} M. Clay mineral amount: 40 mg (2 g·L^{-1}).

3.8. Simulated Effects of BPA Adsorption and Ozonation on Toxicity

Next, 3^3 factorial experimental designs were applied to model the effects of the initial pH, ozonation time, and clay mineral amounts (Table S3). These parameters were varied at three different levels within ranges based on a synthetic analysis of the literature data and some of our previous works. The resulting polynomial regression equations allow describing both BPA adsorption and ozonation processes, along with each growth parameter of *L. minor* (Tables S4–S6). The models elaborated were validated using t-Student and Fisher tests and Snedecor tables for the three variables, with variance of 2 and a 0.95 confidence level ($p < 0.05$) (Table S7).

The main response functions for (*i*) both the adsorption and ozonation processes and (*ii*) the main biomarkers of *L. minor* strongly depend on the individual effects and interactions of all the three parameters considered (Tables S8–S10). At first glance, most of the optima determined appear to be contained within the established variation ranges of the dimensionless parameter [−1, 1] for both clay minerals (Table S11). This confirms the judicious choice of the variation ranges based on a synthetic analysis of the literature related to the pH effect on Mt behavior in aqueous suspensions in the vicinity of the zero-charge pH (pH_{ZC}), the Fe^{2+} precipitation pH, the lowest pKa value of silanols, and the critical micelle concentration of montmorillonite [88,89]. This also demonstrates the interdependence of the pH and Mt amounts in BPA adsorption, ozonation, and their induced toxicity.

The occurrence of optimum response functions clearly demonstrates that both NaMt and Fe(II)Mt require intermediate values of the starting pH, namely around pH 2.8 (X1 = 0), with a contact time around 15 min (X2 = 0) and a clay concentration of ca. 2 g·L^{-1} (X3 = 0), for optimum BPA removal rates (by adsorption and toxicity) and toxicity parameters. This intrinsically includes optimum values of the concentrations of the leached cations released in the liquid media, the zeta potential, and the clay particle size. These three factors are known to govern the dispersion and contact surfaces of clay minerals, which explains the strong correlations between adsorption and ozonation on the one hand and between

these two processes and the induced toxicity on the other. The effects of the initial pH and the clay mineral concentration in the liquid media were more visible when centering the process duration at 15 min (X2 = 0). Thus, eliminating the effects and interactions of this parameter allows for a more accurate prediction of the expected shape of the response surface (Table S10).

Interestingly, the polynomial models of ZP and PS showed the opposite signs for the quadratic term of pH (X1, −1.96 and 3090.5 for NaMt and −7.64 and 4289.1 for Fe(II)Mt). This confirms that optimum pH values of 0.86 and 0.7 for NaMt and 0.80 and 0.10 for Fe(II)Mt during adsorption result in the maximum ZP and minimum PS in the presence of NaMt and Fe(II)Mt (Table S11). All these values are higher than the central level X1 = 0, i.e., beyond pH 3, when a rise in negative charges and Mt lamella dispersion are triggered. This phenomenon is not observed during ozonation, presumably due to the appearance of competitive interactions of BPA derivatives.

As expected, maximum BPA conversion by ozonation corresponds to the minimum values of the fresh weight and chlorophyll *a*/*b* ratio, thus indicating that NaMt-catalyzed ozonation produces more toxic derivatives than the parent molecule. This aligns with the fact that minimum BPA conversion via Fe(II)Mt-catalyzed ozonation corresponds to the maximum values of the fresh weight and chlorophyll *a*/*b* ratio. In other words, under optimum conditions close to the centered values of the parameters, Fe(II)Mt appears to produce less toxicity towards *L. minor* as compared to NaMt.

These different behaviors of the two clay minerals are likely due to the excessive acidity of the liquid media, induced by a combination of (*i*) the acidic nature of Fe(II)Mt, which should favor BPA adsorption, and (*ii*) the excessive production of acidic species by a more active clay catalyst and more pronounced ozonation. This excessive acidity may lead to (*i*) excessive Fe^{2+} loss by leaching, (*ii*) a decay in the clay's surface charge in agreement with the minimum predicted for the zeta potential, and (*iii*) clay catalyst compaction upon the pronounced conversion of -Si-O groups into neutral silanols and a loss in catalytic activity. Here, all saddle-shaped surfaces indicate similar phenomena that involve contrasting individual effects of the initial pH and clay mineral concentration. This phenomenon accounts for opposite influences (*i*) on the zeta potential and particle size on the one hand and (*ii*) on each of the bioindicators of *L. minor* on the other hand. Therefore, this study explains the strong influence of the fate and detrimental impact of the oxidative degradation of organic pollutants in clay-containing ecosystems, which was the main objective of the present work.

In the case of sodium-exchanged montmorillonite (NaMt), the maximum BPA conversion is observed under conditions corresponding to the maximum zeta potential during ozonation, alongside the minimum fresh weight of *Lemna minor* and the minimum chlorophyll *a*/*b* ratio, confirming the degradation of the toxic compound. These optimal conditions for degradation and the reduction of the ecotoxicological impact are consistently accompanied by minimum BPA adsorption onto the clay. In contrast, for Fe(II)Mt, establishing such clear correlations proves more challenging. This difficulty stems from two key factors: firstly, the divalent charge of Fe^{2+}, which promotes a bridging effect between the montmorillonite (Mt) and BPA, as well as potentially between BPA molecules themselves; secondly, the inherent acidity of Fe^{2+}, which simultaneously influences the surface charge distribution, the adsorption process, and the ozonation pathway.

Considering that adsorption is an unavoidable step in the Mt-catalyzed ozonation process, it appears that its contribution to the catalyst's effectiveness is difficult to assess because the pH decrease induced by the formation of acidic species strongly alters the intrinsic Mt dispersion and contact surface and subsequently BPA's interactions with the solid surface. These interactions, in turn, induce direct effects on the very degradation of

adsorbed and non-adsorbed BPA molecules, which should be in equilibrium at each pH with the derivatives' distribution. Therefore, BPA's oxidative degradation can be correlated to the toxicity towards *L. minor* only if all these individual effects and interactions are considered. Investigations are still in progress in this direction. Deeper insights into the pH effect combined with that of the clay mineral concentration are expected to provide valuable data about potential cation transfers and interactions between the dispersed species in correlation with the induced toxicity.

4. Conclusions

This comprehensive research allows an understanding of the fate of bisphenol A in natural clay-containing media and its potential ecotoxicity. The results obtained herein show that the mere presence of clay minerals induces a marked enhancement in bisphenol degradation by ozonation regardless of the exchangeable cations. During adsorption and ozonation, the BPA removal rate varies according to the exchangeable cations of montmorillonite. Fluctuations in the BPA removal yield during adsorption and ozonation significantly influence the toxicity towards *L. minor*. The optimum clay catalyst concentration and initial pH allow achieving maximum BPA degradation rate with minimal oxidative stress and toxicity towards the plant bioindicator. These optimal conditions vary depending on the type of exchangeable cation present. These valuable findings are expected to allow the prediction of the fate and environmental impacts of organic phenolic pollutants according to the natural host media and chemical composition. The resulting scientific tools should contribute to the development of sustainable remediation strategies, envisioning safe and nature-inspired clay-based water treatments.

Supplementary Materials: The following supporting information can be downloaded at https://www.mdpi.com/article/10.3390/environments13050263/s1. Table S1: Changes in chemical composition (wt.%); Table S2: Composition of the growth medium for *Lemna minor* according to the Swedish standard (SIS medium, which is a specific formulation designed to support the growth of the aquatic plant *Lemna minor*); Figure S1: XRD patterns of the starting NaMt without impregnation in acidic media and of its counterpart after acid treatment for 30 min at pH 1; Figure S2: Evolution of the relative absorbance at 275 nm of BPA (a) and at 225 nm (b) in Nanopure water solutions during adsorption on different exchanged montmorillonites; Figure S3: Evolution in time of BPA UV-Vis spectrum in Nanopure water solutions during adsorption on different exchanged montmorillonites; Figure S4: Evolution of BPA UV-Vis spectrum during adsorption onto NaMt adsorbent at various pH levels in Nanopure water solutions; Figure S5: Evolution of BPA UV-Vis spectrum during adsorption onto Fe(II)Mt adsorbent at various pH levels in Nanopure water solutions; Figure S6: Initial pH effect on BPA retention rate via adsorption on NaMt (a) and Fe(II)Mt (b) in Nanopure water at different pH values as observed by HPLC-DAD; Figure S7: Removal rate of BPA by adsorption in the presence of 40 mg (2 $g \cdot L^{-1}$) of NaMt (a) and Fe(II)Mt (b) for solutions at different pH values as assessed through HPLC-DAD; Figure S8: Evolution in time of BPA UV-Vis spectrum during non-catalytic ozonation in Nanopure water solutions; Figure S9: Evolution in time of BPA UV-Vis spectrum during clay-catalyzed ozonation in Nanopure water solutions; Figure S10: Relative absorbance of the 225 nm (a) and 275 nm (b) bands on different catalysts and without catalyst during ozonation in Nanopure water solutions; Figure S11: Effects of clay catalyst addition on the evolution of the relative HPLC peak area ratio (PA/PAo) during adsorption (a) and ozonation (b) in Nanopure water solutions at intrinsic initial pH and room temperature; Figure S12: Time evolution of the initial pH after addition of BPA adsorption supernatant in *L. minor* containing SIS media (a) and after 7 days of contact time (b); Figure S13: Evolution of the frond proportion of *Lemna minor* as reported to the blank (Control) during adsorption (a) and ozonation (b) in the presence of various cation-exchanged montmorillonites; Figure S14: Time evolution of the initial pH after addition of BPA ozonation supernatant in *L. minor*-containing SIS media (a) and after 7 days of contact time (b); Figure S15: Effects of the ozonized mixtures in the presence of different catalysts on the proportions of plant specimens (a)

and fresh weight of *Lemna minor* (b) as reported to the blank sample (Control); Figure S16: Evolution of the content of chlorophyll *a* and chlorophyll *b* during adsorption (a) and ozonation (b); Figure S17: Shape of the response surface for BPA conversion by ozonation with NaMt (a) and FeMt (b), fresh weight of *Lemna minor* exposed to supernatants from ozonation tests with FeMt (c), and zeta potential for BPA ozonation in the presence of NaMt (d) for a medium process duration of 15 min (X2 = 0); Table S3: Parameter levels and ranges for 3^3 factorial experimental designs at T = 25 °C; Table S4: The 3^3 factorial experimental designs for the final pH after BPA adsorption, retention rate, cation amount released in the liquid medium, zeta potential, and particle size; Table S5: The 3^3 factorial experimental designs for the final pH after ozonation with NaMt and Fe(II)Mt, conversion rate, cation amount released in the liquid media, zeta potential, and particle size; Table S6: The 3^3 factorial experiment designs for some *Lemna minor* biomarkers for the ozonation or adsorption mixture with NaMt and Fe(II)Mt followed by filtration through a 45 µm filter; Table S7: Procedures of adequacy tests and variance analysis for the different models elaborated; Table S8: Polynomial model coefficients for some response-functions of some *L. minor* bioindicators after exposure to BPA mixtures obtained after adsorption on NaMt and Fe(II)Mt; Table S9: Polynomial model coefficients for some response functions for NaMt and Fe(II)Mt-catalyzed BPA ozonation and for *L. minor* bioindicators after exposure to ozonized mixtures; Table S10: Polynomial model of response functions including *L. minor* bioindicators after exposure to BPA mixtures after adsorption or ozonation in the presence of NaMt and Fe(II)Mt at X2 = 0; Table S11: Optimum parameters for some response functions during adsorption and ozonation with NaMt and Fe(II)Mt.

Author Contributions: Conceptualization: A.A., D.D. and A.B.; Methodology: A.B., A.A. and D.D.; Software: A.B.; Validation: A.A., D.D. and A.B.; Formal analysis: A.B.; Investigation: A.B.; Data curation: A.B., A.A. and D.D.; Writing—original draft preparation: A.B. and A.A.; Writing—review and editing: A.B. and A.A.; Visualization: A.B. and A.A.; Supervision: A.A. and D.D. All authors have read and agreed to the published version of the manuscript.

Funding: This research received no external funding.

Institutional Review Board Statement: Not applicable.

Informed Consent Statement: Not applicable.

Data Availability Statement: The original contributions presented in this study are included in the article/Supplementary Materials. Further inquiries can be directed to the corresponding authors.

Conflicts of Interest: The authors declare no conflicts of interest.

References

1. Vandenberg, L.N.; Chahoud, I.; Heindel, J.J.; Padmanabhan, V.; Paumgartten, F.J.; Schoenfelder, G. Urinary, circulating, and tissue biomonitoring studies indicate widespread exposure to bisphenol A. *Cienc. Saude Coletiva* **2012**, *17*, 407–434. [CrossRef]
2. Schecter, A.; Malik, N.; Haffner, D.; Smith, S.; Harris, T.R.; Paepke, O.; Birnbaum, L. Bisphenol A (BPA) in U.S. Food. *Environ. Sci. Technol.* **2010**, *44*, 9425–9430. [CrossRef]
3. Campbell, C.G.; Borglin, S.E.; Green, F.B.; Grayson, A.; Wozei, E.; Stringfellow, W.T. Biologically directed environmental monitoring, fate, and transport of estrogenic endocrine disrupting compounds in water: A review. *Chemosphere* **2006**, *65*, 1265–1280. [CrossRef]
4. Daughton, C.G.; Jones-Lepp, T.L. *Pharmaceuticals and Care Products in the Environment: Scientific and Regulatory Issues*; ACS Publications: Washington, DC, USA, 2001.
5. Sánchez-Avila, J.; Bonet, J.; Velasco, G.; Lacorte, S. Determination and occurrence of phthalates, alkylphenols, bisphenol A, PBDEs, PCBs and PAHs in an industrial sewage grid discharging to a Municipal Wastewater Treatment Plant. *Sci. Total Environ.* **2009**, *407*, 4157–4167. [CrossRef] [PubMed]
6. Jackson, J.; Sutton, R. Sources of endocrine-disrupting chemicals in urban wastewater, Oakland, CA. *Sci. Total Environ.* **2008**, *405*, 153–160. [CrossRef] [PubMed]
7. Gómez, M.J.; Martínez Bueno, M.J.; Lacorte, S.; Fernández-Alba, A.R.; Agüera, A. Pilot survey monitoring pharmaceuticals and related compounds in a sewage treatment plant located on the Mediterranean coast. *Chemosphere* **2007**, *66*, 993–1002. [CrossRef]
8. Kuch, H.M.; Ballschmiter, K. Determination of Endocrine-Disrupting Phenolic Compounds and Estrogens in Surface and Drinking Water by HRGC−(NCI)−MS in the Picogram per Liter Range. *Environ. Sci. Technol.* **2001**, *35*, 3201–3206. [CrossRef]

9. Braunrath, R.; Podlipna, D.; Padlesak, S.; Cichna-Markl, M. Determination of bisphenol A in canned foods by immunoaffinity chromatography, HPLC, and fluorescence detection. *J. Agric. Food Chem.* **2005**, *53*, 8911–8917. [CrossRef]
10. Oppeneer, S.J.; Robien, K. Bisphenol A exposure and associations with obesity among adults: A critical review. *Public Health Nutr.* **2014**, *18*, 1847–1863. [CrossRef]
11. Xue, J.; Kannan, P.; Kumosani, T.A.; Al-Malki, A.L.; Kannan, K. Resin-based dental sealants as a source of human exposure to bisphenol analogues, bisphenol A diglycidyl ether, and its derivatives. *Environ. Res.* **2018**, *162*, 35–40. [CrossRef] [PubMed]
12. Barriuso, E.; Calvet, R.; Schiavon, M.; Soulas, G. Les pesticides et les polluants organiques des sols: Transformations et dissipation. *Etude Gest. Sols* **1996**, *3*, 279–295.
13. Azzouz, A.; Mirila, D.-C.; Nistor, D.-I.; Boudissa, F.; Roy, R. Advances in the oxidative degradation of organic pollutants: Prospects for catalyzed oxidation processes targeting total mineralization. In *Advances in Chemistry Research-General Chemistry*; Taylor, J.C., Ed.; Nova Science Publishers: Hauppauge, NY, USA, 2019; Volume 49, p. Chapter ID: 55467.
14. Weber, R.; Watson, A.; Forter, M.; Oliaei, F. Persistent organic pollutants and landfills—A review of past experiences and future challenges. *Waste Manag. Res.* **2011**, *29*, 107–121. [CrossRef]
15. Yong, R.N.; Rao, S.M. Mechanistic evaluation of mitigation of petroleum hydrocarbon contamination by soil medium. *Can. Geotech. J.* **1991**, *28*, 84–91. [CrossRef]
16. Meite, L.; Szabo, R.; Mazellier, P.; de Laat, J. Kinetics of phototransformation of emerging contaminants in aqueous solution. *Rev. Sci. L'eau* **2010**, *23*, 31–39. [CrossRef]
17. Trabelsi, H. *Etude de la Dégradabilité et de la Toxicité des Colorants par Ozonation et Photocatalyse*; Université de Monastir: Monastir, Tunisia, 2014. [CrossRef]
18. Azzouz, A.; Hausler, R.; El-Akhrass, M. Chapter 17—Pesticides and removal approaches. In *Sorbents Materials for Controlling Environmental Pollution*; Núñez-Delgado, A., Ed.; Elsevier: Amsterdam, The Netherlands, 2021; pp. 435–462.
19. Mougin, C.; Chaplain, V.; Rama-Mercier, R.; Sohier, L.; Sigoillot, J.-C.; Asther, M. Utilisation de champignons filamenteux pour la dépollution de sols pollués par des polluants organiques. *Déchets Sci. Tech.* **1996**, *4*, 20–22. [CrossRef]
20. Liao, C.; Liu, F.; Kannan, K. Bisphenol S, a new bisphenol analogue, in paper products and currency bills and its association with bisphenol A residues. *Environ. Sci. Technol.* **2012**, *46*, 6515–6522. [CrossRef] [PubMed]
21. Meeker, J.D.; Ehrlich, S.; Toth, T.L.; Wright, D.L.; Calafat, A.M.; Trisini, A.T.; Ye, X.; Hauser, R. Semen quality and sperm DNA damage in relation to urinary bisphenol A among men from an infertility clinic. *Reprod. Toxicol.* **2010**, *30*, 532–539. [CrossRef] [PubMed]
22. Lassen, T.H.; Frederiksen, H.; Jensen, T.K.; Petersen, J.H.; Joensen, U.N.; Main, K.M.; Skakkebaek, N.E.; Juul, A.; Jørgensen, N.; Andersson, A.-M. Urinary Bisphenol A Levels in Young Men: Association with Reproductive Hormones and Semen Quality. *Environ. Health Perspect.* **2014**, *122*, 478–484. [CrossRef]
23. Metcalfe, C.D.; Metcalfe, T.L.; Kiparissis, Y.; Koenig, B.G.; Khan, C.; Hughes, R.J.; Croley, T.R.; March, R.E.; Potter, T. Estrogenic potency of chemicals detected in sewage treatment plant effluents as determined by in vivo assays with Japanese medaka (*Oryzias latipes*). *Environ. Toxicol. Chem.* **2001**, *20*, 297–308. [CrossRef]
24. Schulte-Oehlmann, U.; Tillmann, M.; Casey, D.; Duft, M.; Markert, B.; Oehlmann, J. Östrogenartige wirkungen von bisphenol a auf vorderkiemenschnecken (Mollusca: Gastropoda: Prosobranchia). *Umweltwissenschaften Schadst.-Forsch.* **2001**, *13*, 319. [CrossRef]
25. Chen, J.; Saili, K.S.; Liu, Y.; Li, L.; Zhao, Y.; Jia, Y.; Bai, C.; Tanguay, R.L.; Dong, Q.; Huang, C. Developmental bisphenol A exposure impairs sperm function and reproduction in zebrafish. *Chemosphere* **2017**, *169*, 262–270. [CrossRef]
26. Gore, A.C.; Chappell, V.A.; Fenton, S.E.; Flaws, J.A.; Nadal, A.; Prins, G.S.; Toppari, J.; Zoeller, R.T. EDC-2: The Endocrine Society's second scientific statement on endocrine-disrupting chemicals. *Endocr. Rev.* **2015**, *36*, E1–E150. [CrossRef] [PubMed]
27. Yuan, M.; Hu, M.; Lou, Y.; Wang, Q.; Mao, L.; Zhan, Q.; Jin, F. Environmentally relevant levels of bisphenol A affect uterine decidualization and embryo implantation through the estrogen receptor/serum and glucocorticoid-regulated kinase 1/epithelial sodium ion channel α-subunit pathway in a mouse model. *Fertil. Steril.* **2018**, *109*, 735–744.e731. [CrossRef] [PubMed]
28. Brown, A.R.; Green, J.M.; Moreman, J.; Gunnarsson, L.M.; Mourabit, S.; Ball, J.; Winter, M.J.; Trznadel, M.; Correia, A.; Hacker, C. Cardiovascular effects and molecular mechanisms of bisphenol a and its metabolite MBP in zebrafish. *Environ. Sci. Technol.* **2018**, *53*, 463–474. [CrossRef]
29. Reis, L.d.P.G.; Lora-Benítez, A.J.; Molina-López, A.M.; Mora-Medina, R.; Ayala-Soldado, N.; Moyano-Salvago, M. Evaluation of the Toxicity of Bisphenol A in Reproduction and Its Effect on Fertility and Embryonic Development in the Zebrafish (*Danio rerio*). *Int. J. Environ. Res. Public Health* **2022**, *19*, 962. [CrossRef]
30. Corrales, J.; Kristofco, L.A.; Steele, W.B.; Yates, B.S.; Breed, C.S.; Williams, E.S.; Brooks, B.W. Global assessment of bisphenol A in the environment: Review and analysis of its occurrence and bioaccumulation. *Dose-Response* **2015**, *13*, 1559325815598308. [CrossRef] [PubMed]
31. Lang, I.A.; Galloway, T.S.; Scarlett, A.; Henley, W.E.; Depledge, M.; Wallace, R.B.; Melzer, D. Association of Urinary Bisphenol A concentration with medical disorders and laboratory abnormalities in adults. *JAMA* **2008**, *300*, 1303–1310. [CrossRef]

32. Pérez-Bermejo, M.; Mas-Pérez, I.; Murillo-Llorente, M.T. The role of the bisphenol A in diabetes and obesity. *Biomedicines* **2021**, *9*, 666. [CrossRef]
33. Seachrist, D.D.; Bonk, K.W.; Ho, S.-M.; Prins, G.S.; Soto, A.M.; Keri, R.A. A review of the carcinogenic potential of bisphenol A. *Reprod. Toxicol.* **2016**, *59*, 167–182. [CrossRef]
34. Bergman, Å.; Heindel, J.J.; Jobling, S.; Kidd, K.; Zoeller, T.R.; World Health Organization. *State of the Science of Endocrine Disrupting Chemicals 2012*; World Health Organization: Geneva, Switzerland, 2013.
35. Diamanti-Kandarakis, E.; Bourguignon, J.-P.; Giudice, L.C.; Hauser, R.; Prins, G.S.; Soto, A.M.; Zoeller, R.T.; Gore, A.C. Endocrine-disrupting chemicals: An Endocrine Society scientific statement. *Endocr. Rev.* **2009**, *30*, 293–342. [CrossRef]
36. Cousins, I.; Staples, C.; Klečka, G.; Mackay, D. A multimedia assessment of the environmental fate of bisphenol A. *Hum. Ecol. Risk Assess.* **2002**, *8*, 1107–1135. [CrossRef]
37. Tijani, J.O.; Fatoba, O.O.; Madzivire, G.; Petrik, L.F. A review of combined advanced oxidation technologies for the removal of organic pollutants from water. *Water Air Soil Pollut.* **2014**, *225*, 1–30. [CrossRef]
38. Im, J.; Löffler, F.E. Fate of bisphenol A in terrestrial and aquatic environments. *Environ. Sci. Technol.* **2016**, *50*, 8403–8416. [CrossRef]
39. Numata, M.; Yarita, T.; Aoyagi, Y.; Yamazaki, M.; Takatsu, A. Investigation of saponification for determination of polychlorinated biphenyls in marine sediments. *Chemosphere* **2005**, *58*, 865–875. [CrossRef] [PubMed]
40. Northcott, G.L.; Jones, K.C. Validation of procedures to quantify nonextractable polycyclic aromatic hydrocarbon residues in soil. *J. Environ. Qual.* **2003**, *32*, 571–582. [CrossRef] [PubMed]
41. Arslan, İ.; Akmehmet Balcioğlu, I.; Tuhkanen, T. Oxidative treatment of simulated dyehouse effluent by uv and near-UV light assisted Fenton's reagent. *Chemosphere* **1999**, *39*, 2767–2783. [CrossRef]
42. Tang, S.; Yuan, D.; Zhang, Q.; Liu, Y.; Zhang, Q.; Liu, Z.; Huang, H. Fe-Mn bi-metallic oxides loaded on granular activated carbon to enhance dye removal by catalytic ozonation. *Environ. Sci. Pollut. Res.* **2016**, *23*, 18800–18808. [CrossRef] [PubMed]
43. Khanna, R.; Konyukhov, Y.; Maslennikov, N.; Kolesnikov, E.; Burmistrov, I. An Overview of Dental Solid Waste Management and Associated Environmental Impacts: A Materials Perspective. *Sustainability* **2023**, *15*, 15953. [CrossRef]
44. Priyadarshanee, M.; Mahto, U.; Das, S. Mechanism of toxicity and adverse health effects of environmental pollutants. In *Microbial Biodegradation and Bioremediation*; Elsevier: Amsterdam, The Netherlands, 2022; pp. 33–53.
45. Zhang, Y.; Wang, Q.; Wang, X.; Xiong, R.; Fu, D.; He, C.; Lai, B.; Ma, J. Enhanced degradation of Bisphenol AF by Fe/Zn modified biochar/ferrate (VI): Performance and enhancement mechanism. *J. Environ. Chem. Eng.* **2023**, *11*, 111582. [CrossRef]
46. Li, L.; Hu, J.; Shi, X.; Fan, M.; Luo, J.; Wei, X. Nanoscale zero-valent metals: A review of synthesis, characterization, and applications to environmental remediation. *Environ. Sci. Pollut. Res.* **2016**, *23*, 17880–17900. [CrossRef]
47. Azzouz, A.; Dewez, D.; Benghaffour, A.; Hausler, R.; Roy, R. Role of Clay Minerals in Natural Media Self-Regeneration from Organic Pollution-Prospects for Nature-Inspired Water Treatments. *Molecules* **2024**, *29*, 5108. [CrossRef]
48. Prabakaran, K.; Li, J.; Anandkumar, A.; Leng, Z.; Zou, C.B.; Du, D. Managing environmental contamination through phytoremediation by invasive plants: A review. *Ecol. Eng.* **2019**, *138*, 28–37. [CrossRef]
49. Han, Y.; Dai, H.; Rong, X.; Jiang, H.; Xue, Y. Research progress of methods for degradation of bisphenol A. *Molecules* **2023**, *28*, 8028. [CrossRef]
50. Boudissa, F.; Mirila, D.; Arus, V.A.; Terkmani, T.; Semaan, S.; Proulx, M.; Nistor, I.D.; Roy, R.; Azzouz, A. Acid-treated clay catalysts for organic dye ozonation—Thorough mineralization through optimum catalyst basicity and hydrophilic character. *J. Hazard. Mater.* **2019**, *364*, 356–366. [CrossRef] [PubMed]
51. Mirilă, D.-C.; Boudissa, F.; Beltrao-Nuñes, A.-P.; Platon, N.; Didi, M.-A.; Nistor, I.-D.; Roy, R.; Azzouz, A. Organic Dye Ozonation Catalyzed by Chemically Modified Montmorillonite K10–Role of Surface Basicity and Hydrophilic Character. *Ozone Sci. Eng.* **2020**, *42*, 517–530. [CrossRef]
52. Djidja, R.; Dewez, D.; Azzouz, A. Norfloxacin Oxidative Degradation and Toxicity in Aqueous Media: Reciprocal Effects of Acidity Evolution on Metal Cations and Clay Catalyst Dispersion. *Int. J. Mol. Sci.* **2025**, *26*, 4347. [CrossRef] [PubMed]
53. Djidja, R.; Dewez, D.; Azzouz, A. Clay-catalyzed ozonation of Norfloxacin—Effects of metal cation and degradation rate on aqueous media toxicity towards *Lemna minor*. *Chemosphere* **2025**, *372*, 144088. [CrossRef]
54. Boudissa, F.; Arus, V.-A.; Foka-Wembe, E.-N.; Zekkari, M.; Ouargli-Saker, R.; Dewez, D.; Roy, R.; Azzouz, A. Role of Silica on Clay-Catalyzed Ozonation for Total Mineralization of Bisphenol-A. *Molecules* **2023**, *28*, 3825. [CrossRef]
55. Tayeb, R.; Ouargli-Saker, R.; Lachachi, K.A.; Zekkari, M.; Hadjel, M.; Azzouz, A. Zeolite 4A-loaded mesoporous SBA-like silicas with improved adsorptive capacity for bisphenol A removal. *Inorg. Chem. Commun.* **2025**, *176*, 114205. [CrossRef]
56. Benghaffour, A.; Azzouz, A.; Dewez, D. Ecotoxicity of Diazinon and Atrazine Mixtures after Ozonation Catalyzed by Na+ and Fe^{2+} Exchanged Montmorillonites on *Lemna minor*. *Molecules* **2023**, *28*, 6108. [CrossRef] [PubMed]
57. Benghaffour, A.; Dewez, D.; Azzouz, A. Correlation of pesticide ecotoxicity with clay mineral dispersion effect on adsorption and ozonation—An approach through impact assessment on *Lemna minor*. *Appl. Clay Sci.* **2023**, *241*, 107001. [CrossRef]

58. Benghaffour, A.; Foka-Wembe, E.-N.; Dami, M.; Dewez, D.; Azzouz, A. Insight into natural medium remediation through ecotoxicity correlation with clay catalyst selectivity in organic molecule ozonation. *Dalton Trans.* **2022**, *51*, 4366–4376. [CrossRef] [PubMed]
59. Foka Wembe, E.N.; Benghafour, A.; Dewez, D.; Azzouz, A. Clay-Catalyzed ozonation of organic pollutants in water and toxicity on *Lemna minor*: Effects of molecular structure and interactions. *Molecules* **2022**, *28*, 222. [CrossRef]
60. Silva, C.A.C.N. Avaliação da Toxicidade aguda do Bisfenol A (BPA) em Espécies Marinhas e Estuarinas Tropicais de Diferentes Grupos Tróficos. Master's Thesis, Universidade Federal do Estado do Rio de Janeiro, Rio de Janeiro, Brazil, 2020.
61. Organization for Economic Cooperation and Development. *Lemna OECD Guidelines for the Testing of Chemicals*; Test No. 221: Sp. growth inhibition test; OECD: Paris, France, 2006.
62. Shahidi, D.; Moheb, A.; Abbas, R.; Larouk, S.; Roy, R.; Azzouz, A. Total mineralization of sulfamethoxazole and aromatic pollutants through Fe^{2+}-montmorillonite catalyzed ozonation. *J. Hazard. Mater.* **2015**, *298*, 338–350. [CrossRef]
63. Bieseki, L.; Bertella, F.; Treichel, H.; Penha, F.; Pergher, S. Acid treatments of montmorillonite-rich clay for Fe removal using a factorial design method. *Mater. Res.* **2013**, *16*, 1122–1127. [CrossRef]
64. Bendou, S.; Amrani, M. Effect of Hydrochloric Acid on the Structural of Sodic-Bentonite Clay. *J. Miner. Mater. Charact. Eng.* **2014**, *2*, 404–413. [CrossRef]
65. Lunardi, C.N.; Gomes, A.J.; Rocha, F.S.; De Tommaso, J.; Patience, G.S. Experimental methods in chemical engineering: Zeta potential. *Can. J. Chem. Eng.* **2021**, *99*, 627–639. [CrossRef]
66. Djidja, R.; Dewez, D.; Azzouz, A. Molecular Interactions of Norfloxacin in Metal-Loaded Clay Suspensions-Effects on Degradation and Induced Toxicity. *Int. J. Mol. Sci.* **2026**, *27*, 459. [CrossRef]
67. Lichtenthaler, H.K.; Buschmann, C. Chlorophylls and carotenoids: Measurement and characterization by UV-VIS spectroscopy. *Curr. Protoc. Food Anal. Chem.* **2001**, *1*, F4. 3.1–F4. 3.8. [CrossRef]
68. Bolt, G.H. Determination of the Charge Density of Silica Sols. *J. Phys. Chem.* **1957**, *61*, 1166–1169. [CrossRef]
69. Sögaard, C.; Funehag, J.; Abbas, Z. Silica sol as grouting material: A physio-chemical analysis. *Nano Converg.* **2018**, *5*, 6. [CrossRef] [PubMed]
70. Pecini, E.M.; Avena, M.J. Measuring the isoelectric point of the edges of clay mineral particles: The case of montmorillonite. *Langmuir* **2013**, *29*, 14926–14934. [CrossRef]
71. Kosmulski, M. The pH dependent surface charging and points of zero charge. X. Update. *Adv. Colloid Interface Sci.* **2023**, *319*, 102973. [CrossRef]
72. Young, T.; Geng, M.; Lin, L.; Thagard, S. Oxidative Degradation of Bisphenol A: A Comparison Between Fenton Reagent, UV, UV/H_2O_2 and Ultrasound. *J. Adv. Oxid. Technol.* **2013**, *16*, 89–101. [CrossRef]
73. Gao, P.; Liu, X.; Guo, Z.; Tournassat, C. Acid-Base Properties of Cis-Vacant Montmorillonite Edge Surfaces: A Combined First-Principles Molecular Dynamics and Surface Complexation Modeling Approach. *Environ. Sci. Technol.* **2023**, *57*, 1342–1352. [CrossRef]
74. Szyper, M.; Zuman, P. Electronic absorption of carboxylic acids and their anions. *Anal. Chim. Acta* **1976**, *85*, 357–373. [CrossRef]
75. Rodríguez, L.F.G.; Zermeño, B.; de la O, K.A.L.; Leyva, E.; Moctezuma, E. Photocatalytic degradation of Bisphenol A: Kinetic studies and determination of the reaction pathway. *J. Appl. Res. Technol.* **2019**, *16*. [CrossRef]
76. Katsumata, H.; Kawabe, S.; Kaneco, S.; Suzuki, T.; Ohta, K. Degradation of bisphenol A in water by the photo-Fenton reaction. *J. Photochem. Photobiol. A Chem.* **2004**, *162*, 297–305. [CrossRef]
77. Xue, L.; Li, Y.; Liu, X.; Liu, Q.; Shang, J.; Duan, H.; Dai, L.; Shui, J. Zigzag carbon as efficient and stable oxygen reduction electrocatalyst for proton exchange membrane fuel cells. *Nat. Commun.* **2018**, *9*, 3819. [CrossRef]
78. Mazellier, P.; Leverd, J. Transformation of 4-tert-octylphenol by UV irradiation and by an H_2O_2/UV process in aqueous solution. *Photochem. Photobiol. Sci.* **2003**, *2*, 946–953. [CrossRef]
79. Deborde, M.; Rabouan, S.; Mazellier, P.; Duguet, J.P.; Legube, B. Oxidation of bisphenol A by ozone in aqueous solution. *Water Res.* **2008**, *42*, 4299–4308. [CrossRef] [PubMed]
80. Mutseyekwa, M.E.; Doğan, Ş.; Pirgalıoğlu, S. Ozonation for the removal of bisphenol A. *Water Sci. Technol.* **2017**, *76*, 2764–2775. [CrossRef]
81. Yun, D.; de Serrano, V.; Ghiladi, R.A. Oxidation of bisphenol A (BPA) and related compounds by the multifunctional catalytic globin dehaloperoxidase. *J. Inorg. Biochem.* **2023**, *238*, 112020. [CrossRef]
82. Porcar-Santos, O.; Cruz-Alcalde, A.; Sans, C. Aqueous oxidation of bisphenol analogues by ozone: Relevance of substituents on reactivity. *J. Environ. Chem. Eng.* **2023**, *11*, 110849. [CrossRef]
83. Yu, J.; Gong, Y.; Nair, P.; Liggio, J.; Peng, H.; Abbatt, J.P.D. Multiphase Ozonolysis of Bisphenol A: Chemical Transformations on Surfaces in the Environment. *Environ. Sci. Technol.* **2024**, *58*, 3931–3941. [CrossRef]
84. Gultekin, I.; Mavrov, V.; Ince, N.H. Degradation of bisphenol-A by ozonation. *J. Adv. Oxid. Technol.* **2009**, *12*, 242–248. [CrossRef]
85. Garoma, T.; Matsumoto, S.; Wu, Y.; Klinger, R. Removal of bisphenol A and its reaction-intermediates from aqueous solution by ozonation. *Ozone Sci. Eng.* **2010**, *32*, 338–343. [CrossRef]

86. Brown, I.D. 14—The Bond-Valence Method: An Empirical Approach to Chemical Structure and Bonding. In *Industrial Chemistry Library*; O'Keeffe, M., Navrotsky, A., Eds.; Elsevier: Amsterdam, The Netherlands, 1981; Volume 2, pp. 1–30.
87. Hawthorne, F.; Schindler, M. Understanding the weakly bonded constituents in oxysalt minerals. *Z. Krist.-Cryst. Mater.* **2008**, *223*, 41–68. [CrossRef]
88. Bergaya, F.; Theng, B.K.G.; Lagaly, G.; Theng, B.K.G.; Lagaly, G. *Handbook of Clay Science*; Elsevier Science and Technology: Amsterdam, The Netherlands, 2006.
89. Sulpizi, M.; Gaigeot, M.-P.; Sprik, M. The Silica–Water Interface: How the Silanols Determine the Surface Acidity and Modulate the Water Properties. *J. Chem. Theory Comput.* **2012**, *8*, 1037–1047. [CrossRef] [PubMed]

Disclaimer/Publisher's Note: The statements, opinions and data contained in all publications are solely those of the individual author(s) and contributor(s) and not of MDPI and/or the editor(s). MDPI and/or the editor(s) disclaim responsibility for any injury to people or property resulting from any ideas, methods, instructions or products referred to in the content.